

Modeling and Performance Analysis of 1.55 μm Quantum Well Edge Emitting Laser Based on InGaN



Md. Jahirul Islam


A thesis submitted in partial fulfillment of the requirements for the degree of Master of Science in the Department of Electrical and Electronic Engineering, Khulna University of Engineering & Technology (KUET).




Department of Electrical and Electronic Engineering
Khulna University of Engineering & Technology
Khulna-920300, Bangladesh.
January, 2012

Declaration

This is to certify that the thesis work entitled "*Modeling and Performance Analysis of 1.55 μm Quantum Well Edge Emitting Laser Based on InGaN*" has been carried out by *Md. Jahirul Islam* in the *Department of Electrical and Electronic Engineering*, Khulna University of Engineering & Technology, Khulna, Bangladesh. According to my knowledge the above thesis work or any part of this work has not been submitted anywhere for the award of any degree or diploma.

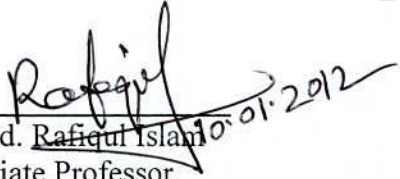

10.01.2012
Signature of Supervisor


10.01.2012
Signature of Candidate

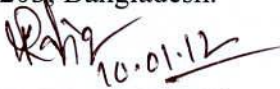
Approval

This is to certify that the thesis work submitted by *Md. Jahirul Islam* entitled "*Modeling and Performance Analysis of 1.55 μm Quantum Well Edge Emitting Laser Based on InGaN*" has been approved by the board of examiners for the partial fulfillment of the requirements for the degree of *Master of Science* in the *Department of Electrical and Electronic Engineering*, *Khulna University of Engineering & Technology*, *Khulna, Bangladesh* in *January 2012*.

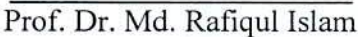
Board of Examiners


Dr. Md. Rafiqul Islam
Associate Professor,
Department of Electrical and Electronic Engineering,
Khulna University of Engineering & Technology,
Khulna-9203, Bangladesh.

Chairman
(Supervisor)

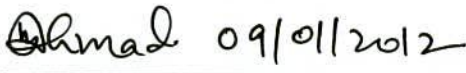

Prof. Dr. Md. Abdur Rafiq
Head of the Department,
Department of Electrical and Electronic Engineering,
Khulna University of Engineering & Technology,
Khulna-9203, Bangladesh.

Member

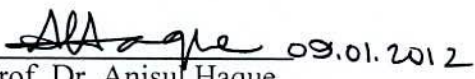

Prof. Dr. Md. Rafiqul Islam
Department of Electrical and Electronic Engineering,
Khulna University of Engineering & Technology,
Khulna-9203, Bangladesh.

Member

Absent


Prof. Dr. Mohiuddin Ahmad
Department of Electrical and Electronic Engineering,
Khulna University of Engineering & Technology,
Khulna-9203, Bangladesh.

Member


Prof. Dr. Anisul Haque
Chairperson,
Department of Electrical and Electronic Engineering,
East West University,
Dhaka, Bangladesh.

Member (External)

Dedicated
To
My Beloved Parents
&
Respected Teachers

Acknowledgements

It is a great pleasure for me to express unbound indebted gratitude to my supervisor Dr. Md. Rafiqul Islam, Associate Professor, Department of Electrical & Electronic Engineering of Khulna University of Engineering & Technology, for his numerous helpful & constructive suggestions, scholastic guidance, constant inspiration & support, valuable advice and kind co-operation for the successful completion of work "*Modeling and Performance Analysis of 1.55 μm Quantum Well Edge Emitting Laser Based on InGaN*". He has always been extremely generous with his time, knowledge and ideas and allowed me great freedom in this research. His enthusiastic approach to research, his endless excitement for laser diode, especially for InGaN based laser and his effervescent personality have made this thesis all the more enjoyable and I am greatly encouraged.

I'm highly grateful to Prof. Dr. Ashraful Ghani Bhuiyan, Dean, Faculty of Electrical & Electronic Engineering, Khulna University of Engineering & Technology who was the pioneer and inspiring person to me. His valuable advice, morality, support and enthusiastic encourage always finds path for me. My cordial thanks is also extended to Prof. Dr. Md. Rafiqul Islam for giving many ideas and for his in-depth knowledge in the field of semiconductor material and laser diode. His helpful discussion about laser made my research easy.

I would like to thank Md. Mahbub Hasan, Md. Rejvi Kaysir and Md. Tanvir Hasan. Many times, they helped me to collect information and ideas related to this research work.

I would also like to thank my family and friends for their encouragement and moral support.

Author

ABSTRACT

Modeling and Performance Analysis of 1.55 μm Quantum Well Edge Emitting Laser Based on InGaN

The advent of research work for longer wavelength 1.55 μm lasers, InGaN advances fast due to its compatible band gap energy and excellent properties. These lasers are well-suited and ideally matched with the existing fiber optic infrastructures as well as bandwidth of the modern ultra speed communication system with substantially lower attenuation, transmission losses, waveform degradation and dispersion penalty. In this thesis, a study is conducted on the design of 1.55 μm InGaN quantum well laser to investigate the effects on various design parameters for the better performance and to deduce an optimum laser structure. The study is separated into stages; it begins with an extensive review on the lasers in chronological order, followed by the development of the laser model with the analysis of band structure interpolation model as well as laser characterization. Next, the thermal and equivalent circuit modeling is presented to investigate the temperature effect and electrical properties of the laser respectively. Careful analysis of the band profile by solving one-dimensional time independent Schrödinger and Poisson's equations using finite difference method is demonstrated. The thermal and circuit-level laser modeling is also developed by solving the respective rate equations. Matlab as well as PSPICE simulation programming languages are employed for numerical analysis.

The simulation and analysis results reveal the energy separation between different band and subbands for quantum well laser. It is observed that the electron density in conduction band is 10^{18}cm^{-3} . It is also found a better efficiency (59%), reduced threshold current density ($1,119\text{A}/\text{cm}^2$), and bias voltage (1.1volts), high optical gain ($9,000\text{ cm}^{-1}$), moderate material gain ($3,660\text{ cm}^{-1}$) and modal gain (45 cm^{-1}). In addition, threshold current, 5.1 mA, output power, 5mW, and slope efficiency, 0.695W/A are obtained. Further understanding of the laser performance with different ambient temperatures the thermal effects has been analyzed. It is found that the threshold current has been increased to 5.5mA at the same ambient. Finally, the circuit level equivalent circuit demonstrates the electrical properties of the laser.

Contents

	PAGE
Title	i
Declaration	ii
Certificate of Research	iii
Dedication	iv
Acknowledgements	v
Abstract	vi
Contents	vii
List of Tables	ix
List of Figures	x
List of Abbreviations	xii
Nomenclature	xiii
CHAPTER I	INTRODUCTION
1.1 Research Background	1
1.2 Approach in this work	3
1.3 Organization of the Thesis	4
1.4 References	5
CHAPTER II	THE LASERS
2.1 Introduction	8
2.2 Chronological Development of Laser	8
2.3 Semiconductor lasers	9
2.3.1 Quantum Well Heterostructure Laser Diode	10
2.4 Key Elements of Semiconductor Lasers	10
2.4.1 P-N Junction	10
2.4.2 Optical resonator	11
2.4.3 Optical Waveguide	12
2.4.4 Optical Transition	12
2.5 Semiconductor Laser: Theory and Operation	13
2.5.1 Excitation (Pumping)	13
2.5.2 Absorption	14
2.5.3 Spontaneous emission	14
2.5.4 Stimulated emission	15
2.5.5 Einstein relations and population inversion	15
2.5.6 Gain, Losses and the Lasing Condition	16
2.5.7 Operation of Laser	17
2.6 References	19

CHAPTER III	MODELING AND SIMULATION METHODOLOGY	
3.1	Introduction	20
3.2	Proposed Physical Model of Laser	20
3.3	Simulation Process	21
3.3.1	Physical Properties	21
3.3.1.1	Composition of In and Ga	21
3.3.1.2	Lattice Constant	22
3.3.1.3	Refractive Index	22
3.3.2	Electronic Energy Bands	24
3.3.2.1	Conduction Band	25
3.3.2.2	Valence Band	26
3.3.3	The fundamental Set of Equations	28
3.3.3.1	Gain	28
3.3.3.2	Efficiency	30
3.3.3.3	I -V Characteristics	31
3.3.3.4	Optical Characteristics	33
3.4	Thermal Modeling of InGaN Based Laser	35
3.5	Equivalent Circuit Modeling of InGaN Based Laser	37
3.6	References	39
CHAPTER IV	RESULTS AND DISCUSSIONS	
4.1	Introduction	43
4.2	Properties of InGaN QW Laser	43
4.2.1	Band Structure	43
4.2.2	Gain of the Laser	46
4.2.3	Efficiency Analysis	48
4.2.4	Output Characteristics	49
4.2.4.1	I -V Characteristics Analysis	49
4.2.4.2	Optical Characteristics Analysis	51
4.3	Thermal Effects on Threshold Current, Output and Power Efficiency	51
4.4	PSPICE Circuit Simulation Results	54
4.5	Comparison of Results	57
4.6	Verification	57
4.7	References	58
CHAPTER V	CONCLUSIONS AND FUTURE WORK	
5.1	Conclusions	61
5.2	Future Works	62
List of Publications on This Thesis		63

LIST OF TABLES

Table No	Description	Page
2.1	Important landmarks in the development of lasers.	9
4.1	The values of the parameters of InN and GaN used in the simulation model.	44
4.2	The InGaN parameters used in the simulation.	46
4.3	Parameters used in PSPICE circuit simulations.	54
4.4	Detail simulation results of InGaN based laser.	58

LIST OF FIGURES

Figure No	Description	Page
1.1	Attenuation wavelength characteristics of glass fiber (Advanced fiber).	2
1.2	Diagram showing the thesis objectives.	3
2.1	Energy band configuration of (a) single quantum well (b) multiple quantum well.	10
2.2	Cross section of a p-n junction in semiconductor lasers.	11
2.3	Carrier injection in a p-n junction under a forward bias.	11
2.4	Cross sectional view of optical waveguide. (a) Index guiding and (b) gain guiding.	12
2.5	A band diagram of three different radiative transition processes in semiconductor.	14
2.6	Key elements in the lasers.	18
2.7	Equivalent circuit of Fig.2.6.	18
3.1	Schematic structure of proposed edge emitting laser.	20
3.2	Composition of In and Ga in $\text{In}_x\text{Ga}_{1-x}\text{N}$.	22
3.3	(a) Lattice constant $a(x)$ of $\text{In}_x\text{Ga}_{1-x}\text{N}$ (b) Lattice constant $c(x)$ of $\text{In}_x\text{Ga}_{1-x}\text{N}$.	22
3.4	Energy band diagram of InGaN quantum well together with refractive index profile.	23
3.5	Active layer thickness vs. optical confinement factor.	34
3.6	PSPICE circuit model of eqn. (3.62)	38
3.7	PSPICE circuit model of eqn. (3.63)	39
3.8	Equivalent circuit model of a single quantum well laser.	39
4.1	Probability distribution corresponding to the lowest eigenvalue.	44
4.2	Probability distribution corresponding to the three eigenvalues.	44
4.3	Electron density profile in conduction band.	45
4.4	Energy of the first conduction subband (C1).	45
4.5	The valence subband dispersion functions of the first conduction and heavy hole bands of quantum well.	46
4.6	Gain vs. photon energy for InGaN based laser at different temperature.	47

4.7	Threshold gain dependency of cavity length.	47
4.8	Material gain variation with photon energy.	47
4.9	Modal gain variation with mirror reflectivity.	47
4.10	External quantum efficiency vs. cavity length, L.	48
4.11	Power conversion efficiency vs. cavity length, L.	48
4.12	Inverse of the external quantum efficiency as a function of cavity length of QW InGaN laser.	49
4.13	Current versus voltage (I-V) characteristics at different temperatures.	50
4.14	Dependence of the threshold current density, J_{th} on the active layer thickness.	50
4.15	Dependence of the threshold current density, J_{th} on the temperature.	50
4.16	Output power from the laser vs. the injection current.	51
4.17	Temperature effect on L-I characteristics of InGaN based laser.	52
4.18	Self-heating effect on L-I characteristic of InGaN based lasers.	52
4.19	Power conversion efficiencies vs. injection current.	52
4.20	Temperature effect on power conversion efficiency.	52
4.21	Thermal resistance variation with heat time constant.	53
4.22	Current vs. voltage relationship for InGaN Laser.	55
4.23	Output power-input current (L-I) characteristic of the proposed laser.	55
4.24	Output transient voltage of the laser.	56
4.25	Turn on delay time.	56

LIST OF ABBREVIATIONS

LASER	Light Amplification by Stimulated Emission of Radiation
OF	Optical fiber
VCSEL	Vertical Cavity Surface Emitting Laser
InGaN	Indium Gallium Nitride
QW	Quantum Well
C	Conduction band
HH	Heavy Hole
LH	Light Hole
LD	Laser Diode
LED	Light Emitting Diode
MQW	Multiple Quantum Well
LI	Light-Current
VI	Voltage-Current
K.P	Kronig-Penney
EDQE	External Differential Quantum Efficiency
PSPICE	Personal Computer Simulation Program with Integrated Circuit Emphasis
ASE	Amplified Spontaneous Emission

NOMENCLATURE

A	Unimolecular recombination coefficients
α_i	Internal loss in the medium,
α_m	The loss due to the mirrors or facets
α_u	Waveguide loss
α_w	Unavoidable signal shot noise loss
α	Absorption coefficient
B	Bimolecular recombination coefficient
B_{12}	Einstein coefficient for absorption
β_{sp}	Spontaneous emission coupling factor
β_A	Unimolecular coupling coefficients
β_B	Bimolecular coupling coefficients
β_C	Auger coupling coefficients
C	Auger recombination coefficients
C_j	Junction depletion capacitance
d	Thickness of active layer
e	Magnitude of a unit charge
E	Electric field intensity
ε	Gain saturation parameter
H	Magnetic field intensity
h	Planck's constant
\hbar	Dirac's constant
$\hbar\omega$	Photon energy
H_{op}	Hamiltonian operator
η_d	External differential quantum efficiency
η_i	Internal quantum efficiency
η_c	Coupling co-efficient
η_p	Power conversion efficiency
L	Length of active layer
L_w	Quantum well thickness
λ	Wavelength
m_b^*	Electron effective mass in barrier

m_w	Electron effective mass in well
n	Electron concentration
n_g	Refractive index of guiding layer
n_c	Refractive index of cladding layer
n_a	Refractive index of active layer
n_s	Refractive index of substrate
N	equilibrium carrier concentration
N_D^+	Ionized donor concentration
N_A^-	Ionized acceptor concentration
p_1	Occupation probabilities in the valence
p_2	Occupation probabilities in the conduction bands
ρ	Charge density
R_m	Mirror reflectivity
R_{th}	Equivalent thermal resistance
S	Photon density
T	Temperature
T_0	Characteristic temperature
τ_r	Radiative recombination lifetime
τ_n	Carrier lifetime
τ_{ph}	Photon lifetime
τ_i	Heat time constant
V_j	Junction voltage
V_d	Build-in potential
x	Indium composition in $In_xGa_{1-x}N$
Φ	The electrostatic potential



INTRODUCTION

1.1 Research Background

LASER is an acronym for Light Amplification by Stimulated Emission of Radiation. It is composed of an active material, which has the optical gain as well as an optical resonator. It is also a highly directional, monochromatic, and coherent light source. The inventions of laser have been proven to be one of the most significant breakthroughs for technology in the last century [1]. The applications of lasers include high speed communications, optical storage like CDs, DVDs, barcode scanners in industrial machines, in printers [2], in medical spectroscopy and imaging, destroying cancer tissues and unnecessary cells in human bodies [1]. We have already entered the era of modern knowledge based society. This needs services like distance learning, self-education through high speed internet facilities and communications between the civilized people in all over the world. Advanced modern societies require hi-tech communication systems, which enormously increases the amount of information transported [3]. Optical fiber communication system overcomes the problems associated with constraints of noise, amount of signal power transmission, interference between RF electromagnetic and other networks. It provides a cost affordable system, high frequency (up to 10^{16} Hz) and large amounts of upstream and downstream bandwidth [4], substantially lower transmission losses [3].

The recent telecommunication industries for medium and long-distance networks (>2 km) rely on lasers operating close to $1.3 \mu\text{m}$ and $1.55 \mu\text{m}$ [4]. The total attenuation at $1.55 \mu\text{m}$ is the lowest. The waveform degradation and the dispersion penalty are lower [5-6] for this wave length. The main advantage of this wavelength range is that, for the optical fiber communications the fibers have a minimum loss (shown in Fig.1.1) around this wavelength range [7] and it is eye-safe wavelength [8]. Therefore the laser diodes operating in this range have a main application in optical fiber communication [1].

The existing materials used to design $1.55 \mu\text{m}$ lasers are ternary, quaternary and quintuplet elements alloy. To reach such a wavelength, the choice of active region has been conscious

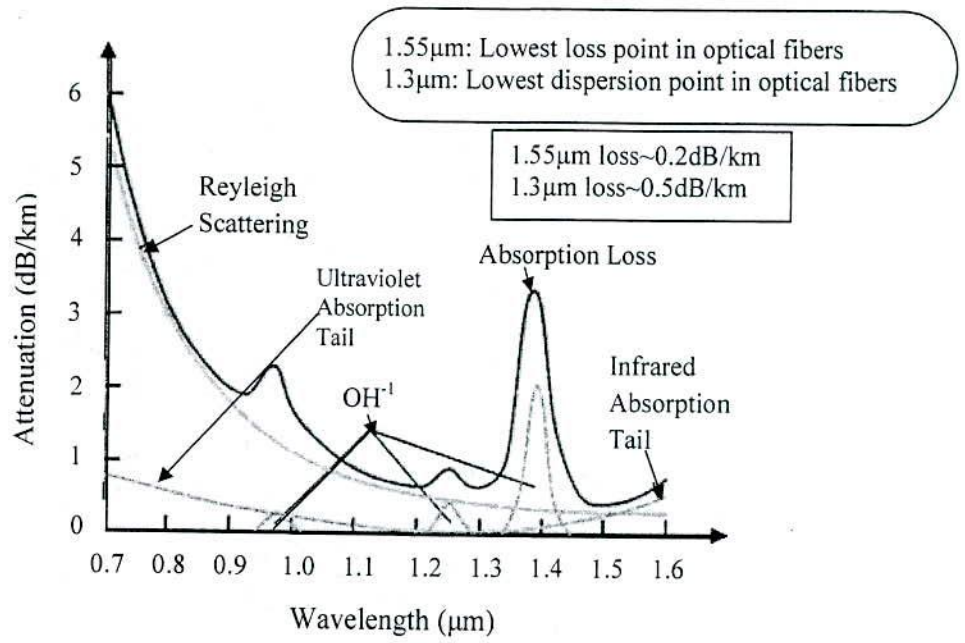


Fig.1.1. Attenuation wavelength characteristics of glass fiber (Advanced fiber) [7].

of the materials including InGaAs/InGaAsP, AlGaInAs, GaInNAsSb/GaAs and GaInAsSb/GaNAs [9-12]. For shorter wave lengths Sandra et al. [13] and Alias et al. [14] described the laser performance using AlGaInAs-InP and InGaAsP respectively. InGaAsP based VCSELs [14] are also found for 1.55 μm lasers. Using mode-locked laser diodes [1] lasers operating at 1.55 μm can be achieved. Ternary, quaternary, and quintuplet materials are difficult to grow with constituent elements due to the necessity of many precursors and creates lasing problem. However, the InGaAs/InGaAsP system has the disadvantage that the conduction band discontinuity ΔE_c is much smaller than the valence band discontinuity ΔE_v , preventing a strong localization of the electrons [15]. These difficulties lead to degrade the quality of the material which reduces the device performance and lifetime.

During the last few years the interest in InN based semiconductor alloys has been remarkable [16]. The III-nitride alloy system allows to extend the fundamental bandgap over a wider region (0.7 eV for InN to 6.2 eV for AlN) [17-18]. In addition, the direct wide-band gap range (0.7 – 6.2 eV), low electron effective mass, high theoretical mobilities, high absorption, high peak saturation velocities, and radiation hardness [19] makes this material system very important subject matter for optoelectronic and microelectronic devices [20]. Incorporation of small amount of Ga in InN will make possible to obtain $\text{In}_x\text{Ga}_{1-x}\text{N}$ with band gap energy of

0.8 eV, which is compatible with the 1.55 μm laser. Therefore, 1.55 μm lasers using InGaN is a promising solution for the future ultra modern communication systems [1].

InGaN edge emitting lasers have simpler construction with a double-heterostructure. It has a thin region of semiconductor with a smaller energy gap sandwiched between two oppositely doped semiconductors with wide bandgap energy. InGaN based 1.55 μm laser is less studied compared with commercialized laser diodes. Piprek et al. [21], Nakamura et al. [22] and Thahab et al. [23-24] only analyze the threshold behavior, mode gain, output power, slope efficiency and electron density profile. To the best of the author knowledge, there are no detail design simulations including band structure calculation, equivalent circuit modeling and thermal effects analysis.

1.2 Approach in this work

Due to the challenges in the InGaN material system for future laser sources, it is imperative to take an iterative approach to successfully develop a high-performance InGaN laser diodes. This iterative process is divided into the following tasks (shown by chart in Fig.1.2), most of which are to be pursued simultaneously.

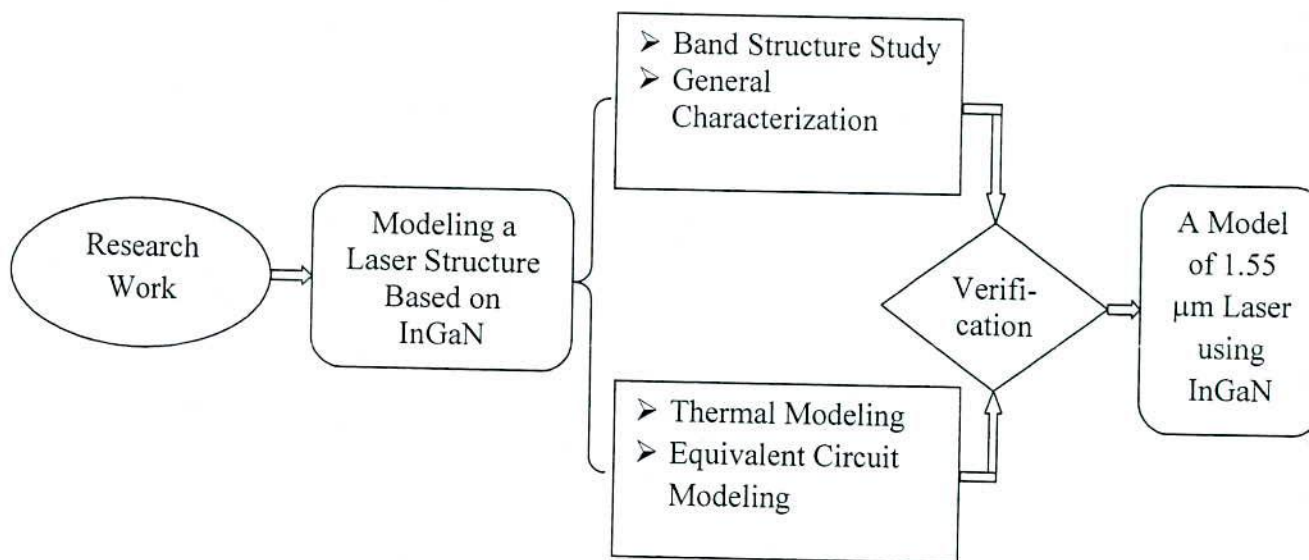


Fig.1.2. Diagram showing the thesis objectives.

The main objective of this thesis is to develop an edge emitting InGaN based quantum well laser structure. The optical reflectivity of the guiding layers as well as the cladding layers also optimized for maximum light reflection and output. The band energy profiles, wave functions for conduction band and valence band are calculated by solving Poisson's and Schrödinger

equations using finite difference method. It is necessary to evaluate the voltage-current (V-I) characteristics, threshold current behavior, gain and its temperature dependency, external quantum efficiency and power conversion efficiency [25] for the laser characterization.

In addition, the study of thermal modeling is also imperative as it discusses on the thermal conductivities of the active region for determining the maximum power [26], diode thermal resistance and self-heating effect of the lasers. In this thesis, a thermal modeling for 1.55- μm quantum-well lasers (QWLs) using InGaN as a promising candidate has been shown. This model is based on the standard laser rate equations and a thermally dependent empirical offset current. It mainly focuses on the dependency of injection current and efficiency on temperature. It also includes thermal effects, temperature-dependent threshold current and output power roll-over at different ambient temperatures.

Furthermore, the equivalent circuit modeling is very necessary to realize practical InGaN based laser diodes. In this thesis a Circuit-Level Laser model has been developed by solving rate equations. Then the electrical performance of the laser has been evaluated using PSPICE.

Finally, a comparative study of the results obtained from these different models as well as the existing available lasers has been shown. Therefore, a comprehensive analysis is presented for the proposed laser structure and finally the performance has been evaluated to optimize the parameters. The outcome of this work will enable us to fabricate the future InGaN based 1.55 μm laser.

1.3 Organization of the Thesis

Modeling and Performance Analysis of 1.55 μm quantum well edge emitting laser based on InGaN is presented in this thesis. The study is separated into several chapters. The background information, present status of 1.55 μm lasers and scope of thesis work on these lasers is presented in Chapter I. It also gives an overview of the potentiality of InGaN materials and the technological over view with the help of a flow chart.

Chapter II begins with the basic concepts necessary for a better understanding of optical laser. The chronological developments, basic theories and operations of laser are explained briefly.

The proposed physical model of the laser is presented in chapter III. The mathematical modeling, theories and characteristics analysis methods are described in this chapter. For the band structure analysis, one dimensional Schrödinger equation has been solved using finite

difference method. Mathematical analysis of the threshold current, gain and efficiency are explained clearly. The thermal modeling and equivalent circuit modeling have been presented.

Chapter IV deals with the results obtained from the mathematical model. The electronic energy band profiles for conduction and valence band has been shown. General laser characteristics and parameter optimization are described here. Results obtained from equivalent circuit modeling as well as thermal modeling are also presented in this chapter. Consistency of these results has shown finally. This chapter also contains a verification of the results with published results.

A detail summarization of the work presented in this thesis has been illustrated in chapter V. A comprehensive suggestion for future works is also presented in this chapter.

1.4 References

- [1] Martijn Jan Resie Heck, "Ultrafast integrated semiconductor laser technology at 1.55 μm " Eindhoven : Technische Universiteit Eindhoven, ISBN 978-90-386-1694-0, 2008.
- [2] Takahiro Numai, "Fundamentals of Semiconductor Lasers", Springer-Verlag New York Inc., ISBN 0387-40836-3, 2004.
- [3] Seok Hun Hyun, "Design Of High-Speed Cmos Laser Driver Using a Standard CMOS Technology for Optical Data Transmission", Atlanta, GA 30332, November, 2004.
- [4] Manish Mehta, Danny Feezell, David A. Buell, Andrew W. Jackson, Larry A. Coldren, and John E. Bowers, "Electrical Design Optimization of Single-Mode Tunnel Junction-Based Long-Wavelength VCSELs," IEEE Journal of Quantum Electronics, Vol. 42, No. 7, pp. 675-682, July 2006
- [5] K. Uomi, A. Murata, S. Sano, R. Takeyari, A. Takai, "Advantage of 1.55 μm InGaAs/InGaAsP MQW-DFB lasers for reducing waveform degradation and dispersion penalty for 2.5 Gb/s long-span normal fiber transmission", IEEE Photonics Technology Letters, Vol. 4, No. 6, pp. 657 – 660, Jun 1992.
- [6] K. Uomi, A. Murata, S. Sano, R. Takeyari, A. Takai, "Advantages of 1.55- μm InGaAs/InGaAsP MQW-DFB lasers for 2.5-Gb/s longspan normal fiber transmission", OSA/OFC 1992.
- [7] Jasprit Sing, "Semiconductor Devices: Basic Principles", ISBN-13: 978-0471362456, July 2000.

- [8] O.P. Kowalski, M. Silver, S. McMaster, D. A. Yanson, B. C. Qiu, S. D. McDougall, J. H. Marsh, "High Power 1.55 μm Laser Diode Sources With High Transverse Beam Quality", 1st EMRS DTC Technical Conference, Edinburgh, 2004.
- [9] P. John Loehr and Jasprit Singh, "Theoretical Studies of the Effect of Strain on Performance of Strained Quantum Well Lasers Based on GaAs and InP Technology", IEEE Journal of Quantum Electronics, Vol. 27, No. 3, pp.708 – 716, March 1991.
- [10] L. Lynford Goddard, R. Seth Bank, A. Mark Wistey, B. Homan Tuen, Rao Zhilong, and S. James Harris, "Recombination, gain, band structure, efficiency, and reliability of 1.5 μm GaInNAsSb/GaAs lasers", Journal of Applied Physics, Vol. 97, No. 8, pp. 083101-15, April 2005.
- [11] L. Lynford Goddard, R. Seth Bank, A. Mark Wistey, B. Homan Yuen, S. James Harris Jr, "High performance GaInNAsSb/GaAs lasers at 1.5 μm ", Proceedings of SPIE Vol. 5738, SPIE, Bellingham, WA, 2005.
- [12] P. Robart Sarzala and Wlodzimierz Nakwaski, "GaInNAsSb/GaNAs quantum-well VCSELs, Modeling and physical analysis in the 1.50- 1.55 μm wavelength range", Journal of Applied Physics, Vol. 101, No. 7, pp. 073103-7, April 2007.
- [13] Sandra R. Selmic, Tso-Min Chou, JiehPing Sih, Jay B. Kirk, Art Mantie, Jerome K. Butler, David Bour, and Gary A. Evans, "Design and Characterization of 1.3- μm AlGaInAs-InP Multiple-Quantum-Well Lasers", IEEE Journal on Selected Topics in Quantum Electronics, Vol. 7, No. 2, pp. 340 – 349, March/April 2001.
- [14] Mohd Sharizal Alias, Burhanuddin Kamaluddin and Muhamad Rasat Muhamad, "1.55 μm Vertical-Cavity Lasers Modeling and Simulation", Solid State Science and Technology, Vol. 13, No 1 & 2, pp. 39-45, 2005.
- [15] S. W. Park, "Threshold Current Density and Differential Gain in InGaAs/InGaAlAs Strained Quantum Well Lasers", J. of the Korean Phys. Soc., Vol. 30, No. 2, pp. 280-285, April 1997.
- [16] M. Gunes, N. Balkan, E. Tiras, S. Ardali, A. O. Ajagunna, E. Iliopoulos, and A. Georgakilas, "Superconductivity in MBE grown InN", Phys. Status Solidi C, Vol. 8, No. 5, pp. 1637–1640, May 2011.
- [17] J. Wu and W. Walukiewicz, "Band gaps of InN and group III nitride alloys", Superlattices and Microstructures, Vol.34, Vo.1-2, pp.63–75, July/Aug 2003.
- [18] J. Wu, "When group-III nitrides go infrared: New properties and perspectives", Journal of Applied Physics, Vol. 106, No. 1, pp. 011101, July 2009.

- [19] N. Faleev , B. Jampana , A. Pancholi , O. Jani, H. Yu, I. Ferguson , V. Stoleru , R. Opila, and C. Honsberg, "High quality InGaN for photovoltaic applications: Type and spatial distribution of crystalline defects and "phase" separation", Proc. of 33rd IEEE Photovoltaic Specialists Conference, May 2008.
- [20] S. -H. Yena, B. -T. Lioub, M. -L. Chena, Y. -K. Kuo, "Piezoelectric and thermal effects on optical properties of violet-blue InGaN lasers", Proc. SPIE, Vol. 5628, pp. 156-163, Jan 2005.
- [21] Joachim Piprek, R. Kehl Sink, Monica A. Hansen, John E. Bowers and Steve P. DenBaars, "Simulation and Optimization of 420 nm InGaN/GaN Laser Diodes", Physics and Simulation of Optoelectronic Devices VIII, SPIE Proc. 3944, 2000.
- [22] Shuji Nakamura, Masayuki Senoh, Shin-ichi Nagahama, Naruhito Iwasa, Toshio atsushita, and Takashi Mukai, "Blue InGaN-based laser diodes with an emission wavelength of 450 nm", Applied Physics Letter 76, pp. 22, 2000.
- [23] S. M. Thahab, H. Abu Hassan, Z. Hassan, "Performance and optical characteristic of InGaN MQWs laser diodes", Optics Express, Vol. 15, No. 5, pp. 2380-2390, March 2007.
- [24] S. M. Thahab, H. Abu Hassan, and Z. Hassan, "Performance of InGaN/GaN Laser Diode Based on Quaternary Alloys Stopper and Superlattice Layers", World Academy of Science, Engineering and Technology 55, pp. 11-14, 2009.
- [25] Shun Lien Chuang, "Optical Gain of Strained Wurtzite GaN Quantum-Well Lasers", IEEE Journal of Quantum Electronics, Vol. 32, No. 10, pp. 1791 – 1800, October 1996.
- [26] T. M. Tritt, "Thermal Conductivity: Theory, Properties, and Applications (Physics of Solids and Liquids)", Springer, ISBN: 0306483270, May 2005.

THE LASER

2.1 Introduction

Laser diodes have been proven to be some of the most significant breakthroughs for human technology. The modeling and simulation of lasers require a clear and in-depth knowledge on the basic theory and operation of the device. This chapter attempts to give a brief overview of chronological development, theory and operation of lasers. The discussions on the key elements such as active material, optical resonator, waveguides and transitions are also presented. The operating principle and necessary conditions for laser operation are explained briefly. This principle describes the amplification of light energy using gain medium. Finally, the pumping, absorption, emission and population inversion for the laser medium has been discussed.

2.2 Chronological Development of Laser

The first scientist who put forward a plausible theory about light was Newton (1642-1727). This theory is known as 'Corpuscular Theory'. Concurrently the 'Wave Theory of Light' was postulated by Huygens. Albert Einstein, with the help of Plank's Quantum Theory of black body radiation, satisfactorily explained the effect of wave theory [1]. He explained that light energy consisted of photons. In 1917, he also established the existence of 'Stimulated Emission' in black body radiation. This concept of stimulated emission later became the backbone of laser physics [2]. In 1956, Malcom W. P. Strandberg of Massachusetts Institute of Technology came up with the idea of designing a two-level, solid state maser. By the end of 1956, H. Scovil, G. Feher and H. Seidd from Bell Labs devised the first maser equipment called Bloembergen's Equipment [3]. Around that time, work on 'Optical Masers' was also going on elsewhere in the world. The semiconductor maser was patent by another two Japanese scientists, Y. Watnabi and J. Ishizawa in 1957 [3]. A soviet researcher V.A. Fabricant and his associates had also been working on stimulated emission of light, throughout the fifties [3]. By this time, optical engineers, scientists and enthusiastic 'student

world' had started clamoring for changing the name of 'this branch of optics' from optical Maser to 'Laser'. So, the name MASER vanished from the scene and the process of light amplification began to be known, popularly, as LASER. In 1960, Maiman successfully demonstrated the operation of laser, for the first time, using a ruby crystal. Shortly after that Javan and his team made the first gas laser, namely, the He-Ne laser [2-3]. The next landmarks for lasers development are shown in table 2.1.

Table 2.1: Important landmarks in the development of lasers

Year	Scientist	Principle/Breakthrough
1961	Javan, Bennet and Harriot	Helium –Neon Laser
1961	Johnson and Nassau	Neodymium Laser
1962	Hall	Semiconductor Laser
1963	Patel	Carbon Dioxide Laser
1964	Bridges	Argon Ion Laser
1966	Silfvast, Fowels and Hopkins	Helium Cadmium Laser
1966	Sorokin and Lankard	Tunable Dye Laser
1975	J. van der Ziel et al.	Quantum Well laser
1976	Madey et al.	Free electron Laser
1979	Walling et al.	Alexandrite Laser
1985	Mathews et al.	X-Ray Laser

2.3 Semiconductor lasers

The semiconductor laser diode is a forward-bias p-n junction, just like the LED. However, the structure appears similar to the LED as far as the electron and holes are concerned, it is quite different from the view point of the photons. As in the case of the LED, electrons and holes are injected into an active region during forward bias condition. On the other hand, these electrons and holes recombine radiatively via the stimulated emission process to emit photons in lasers. Semiconductor lasers are comprised of a large group of binary, ternary, and quaternary elements from Groups III-V from the periodic table such as GaN, AlGaN, InGaAsP, InGaAs, InGaN, GaAs. There are several types laser structures including Edge emitting laser, Vertical cavity surface emitting laser (VCSEL), Quantum cascade laser, Hybrid silicon laser are available. The physical structure of quantum well hetero structure is described in the next section.

2.3.1 Quantum Well Heterostructure Laser Diode

A quantum well is often realized with a thin layer of a semiconductor medium, embedded between other semiconductor layers of wider band gap. Semiconductor quantum wells are used in the active regions of the laser diodes. The electrons and holes are confined in the quantum well and thus increase gain, absorption and reduce density of states. For a rectangular profile, the density of states is constant within certain energy intervals as shown in Fig.2.1. The amount of optical gain or absorption further increases using multiple quantum wells (MQWs), with a spacing to avoid overlap of the corresponding wave functions.

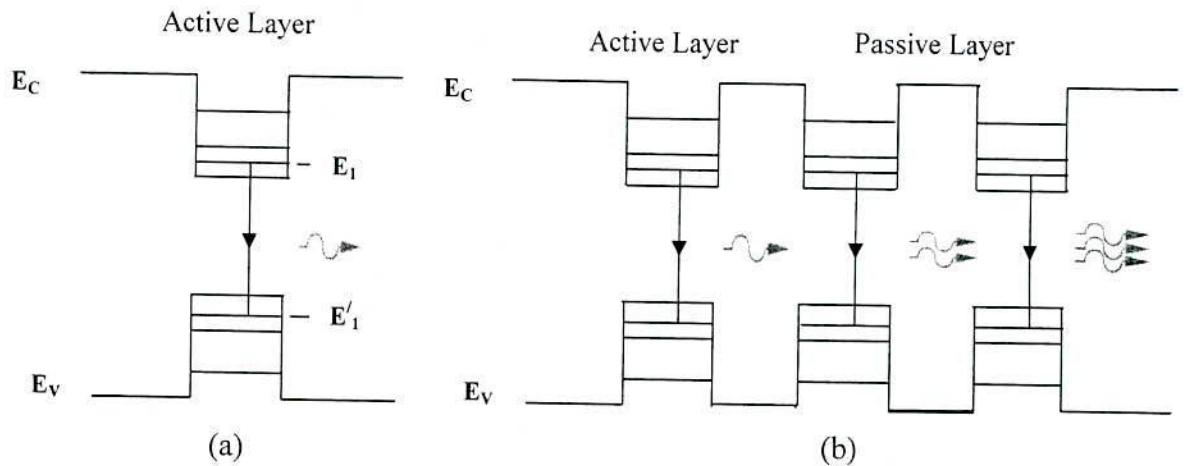


Fig. 2.1. Energy band configuration of (a) single quantum well (b) multiple quantum well.

2.4 Key Elements of Semiconductor Lasers

The basic elements that comprise a semiconductor laser include an active material, optical waveguide and resonator. This section describes the essential elements of lasers one by one.

2.4.1 P-N Junction

In semiconductor lasers, the active layers are placed inside the p-n junctions to inject the carriers. Applying a forward bias voltage across this p-n junction, the electrons are injected from the n-cladding layer while the holes are injected from the p-cladding layer into the active layer as shown in Fig.2.2. When the population inversion is generated by the carrier injection, net stimulated emission is obtained. It is noted that the impurities are often undoped in the active layers to achieve high radiation efficiency. However, in these layers, there are background carriers whose concentrations depend on epitaxial growth methods. The active layers are not

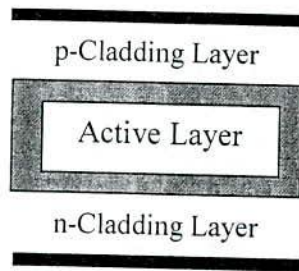


Fig. 2.2. Cross section of a p-n junction in semiconductor lasers.

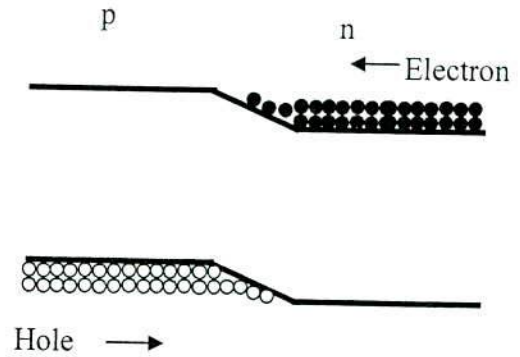


Fig. 2.3. Carrier injection in a p-n junction under a forward bias.

ideal intrinsic semiconductors. If the doping is done by adding impurities in the active layers, the injected carriers combine with the impurities. Then the carrier lifetime is reduced, and the modulation speed is enhanced. The carrier injection in a p-n junction under a forward bias is shown in Fig.2.3. The recombination of the injected carriers and the impurities do not contribute to laser transitions, which decrease the radiation efficiency. Thus, the active layers are sometimes intentionally doped to achieve high-speed modulations so long as the radiation efficiency is not highly degraded.

2.4.2 Optical resonator

The optical resonator, or optical cavity, is two parallel mirrors, placed around the gain medium which provides feedback of the light. The mirrors are given optical coating which determine their reflective properties. Typically one will be a high reflector and the other will be a partial reflector. The latter is called the output coupler, because it allows some of the light to leave the cavity to produce the laser's output beam. Light from the medium, produced by spontaneous emission, is reflected by the mirrors back into the medium, where it may be amplified by stimulated emission. The light may reflect from the mirrors and thus pass through the gain medium many hundreds of times before exiting the cavity. In more complex lasers, configurations with four or more mirrors forming the cavity are used. The design and alignment of the mirrors with respect to the medium is crucial to determining the exact operating wavelength and other attributes of the laser system. Other optical devices, such as spinning mirrors, modulators, filters and absorbers may be placed within the optical resonator, to produce variety of effects on the laser output, such as altering the wavelength of

operation or the production of pulses of laser light. Some lasers do not use an optical cavity, but instead rely on very high optical gain to produce significant amplified spontaneous emission (ASE) without needing feedback of the light back into the gain medium. Such lasers are said to be super luminescent, and emit light with low coherence but high bandwidth. Since they do not use optical feedback, these devices are often not categorized as lasers.

2.4.3 Optical Waveguide

In the semiconductor lasers, only the active layer has the optical gain, and it is extremely inefficient to amplify a beam. Therefore, to amplify lights efficiently, optical waveguides are indispensable for semiconductor lasers. It should be noted that optical fibers are also representative of optical waveguides.

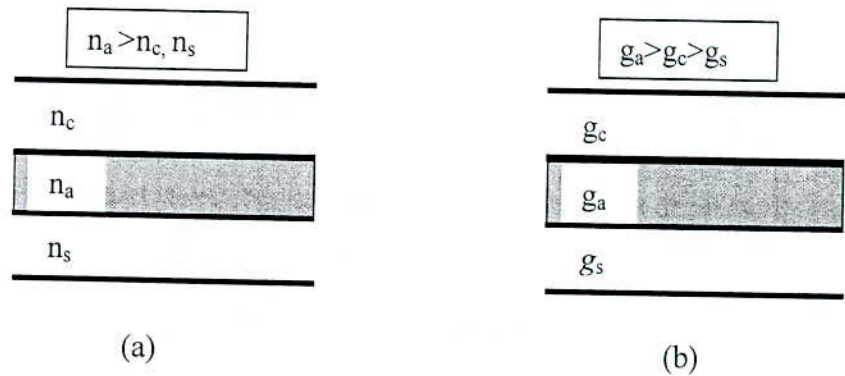


Fig.2.4. Cross sectional view of optical waveguide (a) Index guiding and (b) gain guiding.

Figure 2.4. shows cross-sectional views of the optical waveguides. According to the operating principles, optical waveguides are divided into index guiding waveguides and gain guiding ones. In index guiding waveguides, a light is confined to a high refractive index region, which is surrounded by low refractive index regions. In Fig.2.4 (a), only if the refractive indexes n_a , n_c , and n_s satisfy $n_a > n_c, n_s$ a light is confined to a region with n_a . The gain guiding waveguides use a property that only a gain region amplifies a light, and a light seems to propagate in the gain region. In Fig.2.4 (b), a light is confined to a region with the optical gain, g_a , which is larger than g_c and g_s .

2.4.4 Optical Transition

Among energy states, the state with the lowest energy is most stable. Therefore, the electrons in semiconductors tend to stay in low energy states. If they are excited by thermal energy, light, or electron beams, the electrons absorb these energies and transit to high energy states.

These transitions of the electrons from low energy states to high energy states are called excitations. High energy states, however, are unstable. As a result, to take stable states, the electrons in high energy states transit to low energy states in certain lifetimes. These transitions of the excited electrons from high energy states to low energy states are referred to as relaxations. In semiconductors, the transitions of electrons from high energy states to low energy states are designated recombinations of the electrons and the holes. In the recombinations of the electrons and the holes, there are radiative recombinations and nonradiative recombinations. The radiative recombinations emit photons, and the energies of the photons correspond to a difference in the energies between the initial and final energy states related to the transitions. In contrast, in the nonradiative recombinations, the phonons are emitted to crystal lattices or the electrons are trapped in the defects, and the transition energy is transformed into forms other than light.

2.5 Semiconductor Laser: Theory and Operation

The fundamental principles of laser action and an overview of the theory behind semiconductor laser diodes are provided in this section. Specific details of some of the mathematical equations upon which the electrical semiconductor models are based are also discussed.

2.5.1 Excitation (Pumping)

Luminescence due to optical excitation (pumping) is photoluminescence, which is widely used to characterize materials. Optical excitation is also used to pump dye lasers and solid state lasers. When the photon energy of the pumping light is $\hbar\omega_1$ and that of the luminescence is $\hbar\omega_2$, the luminescence with $\hbar\omega_2 < \hbar\omega_1$ is called Stokes luminescence and that with $\hbar\omega_2 > \hbar\omega_1$ is designated anti-Stokes luminescence. Luminescence caused by electrical excitation is electroluminescence, which has been used for panel displays. In particular, luminescence by current injection is called injection-type electroluminescence; it has been used for light emitting diodes (LEDs) and semiconductor lasers or laser diodes (LDs). In such injection-type optical devices, the carriers are injected into the active layers by forward bias across the p-n junctions. Note that the current (carrier) injection is also considered the excitation, because it generates a lot of high energy electrons.

2.5.2 Absorption

The absorption depicted in Fig.2.5 (a) is a process that the electron transits from a lower energy state to a higher one by absorbing energy from the incident light. Because this transition is induced by the incident light, it is sometimes called induced or stimulated absorption. When a light is incident on a material, the stimulated emission and the absorption simultaneously take place. The spontaneous emission and light amplification by stimulated emission is illustrated in Fig.2.5 (b) and (c) respectively. In thermal equilibrium, there are more electrons in a lower energy state than in a higher one, because the lower energy state is more stable than the higher one. Therefore, in thermal equilibrium, only the absorption is observed when a light is incident on a material.

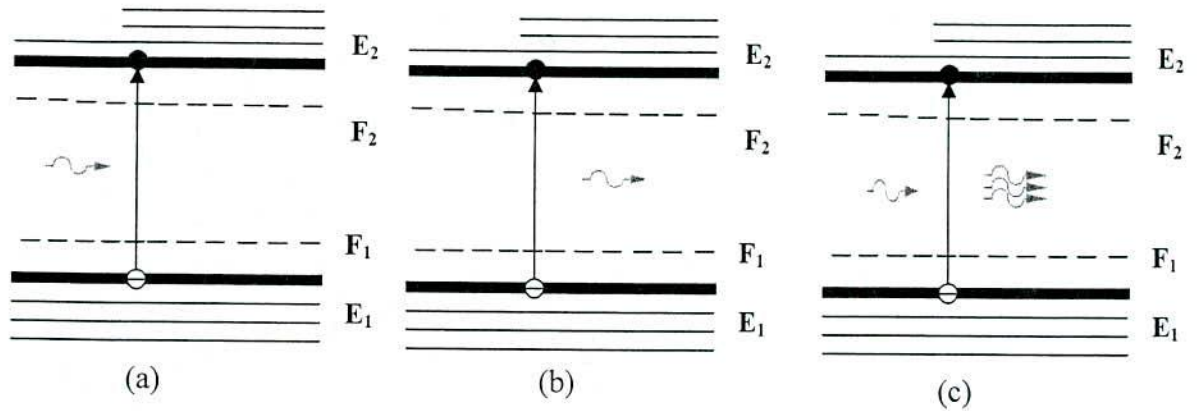


Fig.2.5. Band diagram of three different radiative transition processes in semiconductor.

2.5.3 Spontaneous Emission

In lasers, light is first produced by spontaneous emission, where electrons in the conduction band spontaneously recombine with holes in the valence band to emit photons of equal energy ($E_{\text{electron}} - E_{\text{hole}} = E_g = h\nu$). This initial emission (below threshold) then induces stimulated emission. LEDs, on the other, rely solely on spontaneous emission for device performance. The rate of spontaneous emission, R , is proportional to the product of electron and hole concentrations.

$$R = -\frac{dn}{dt} = -\frac{dp}{dt} = Bnp \quad (2.1)$$

Here, n is the concentration of free electrons, p is the concentration of holes, and B is the bimolecular recombination coefficient.

This can also be expressed in terms of the equilibrium carrier concentrations (n_0, p_0).

$$R = B(n_0 + p_0)\Delta nt \quad (2.2)$$

The rate of change in concentration, $\Delta n(t)$, is an exponential with a characteristic rise time equal to the carrier lifetime, and Δn_0 is the steady state excess electron concentration.

$$\Delta n(t) = \Delta n_0 e^{-B(n_0+p_0)t} \quad \text{and} \quad \tau = \frac{1}{B(n_0+p_0+\Delta n)}$$

2.5.4 Stimulated Emission

If an incident photon “couples” with an electron it can cause the electron to fall back into the valence band. This “coupling” is somewhat analogous to sympathetic resonance in mechanical or acoustical systems. In our case, an incoming photon (emitted via spontaneous emissions) resonantly couples with an energized electron of the same frequency and phase. As the electron falls to the valence band it emits a photon. It is vital to the operation of LDs that the emitted photon is coherent with the incident photon and it has the same direction and phase. The rate of this stimulated emission is dictated by a process completely analogous to stimulated absorption, only this time there is a stimulated emission constant B_{21} which relates to transitions from the conduction to the valence band and is given by [4]

$$R_{\text{emission}} = B_{21} p_1 (1 - p_2) \rho(\hbar\omega) \quad (2.3)$$

Where, p_1 and p_2 are the occupation probabilities in the valence and conduction bands respectively, B_{12} is the Einstein coefficient for absorption, and ρ is the density of photons equal to the transition energy. These processes are really just reverses of each other; stimulated emission is the reverse of stimulated absorption, with the added advantage that stimulated emission multiplies the number of photons and thus provides gain.

2.5.5 Einstein Relations and Population Inversion

All the three of the processes described above (absorption, spontaneous emission, and stimulated emission) are related. This interrelation helps us understand the process of lasing. Consider a system with two energy levels E_1 and E_2 . In equilibrium, the rate of upward transitions must equal the rate of downward transitions, and the populations of each energy level (N_1, N_2) are related by Boltzmann statistics [4]

$$\frac{N_1}{N_2} = \frac{g_{D1} \exp\left(\frac{-E_1}{kT}\right)}{g_{D2} \exp\left(\frac{-E_2}{kT}\right)} = \frac{g_{D1}}{g_{D2}} \exp\left(\frac{E_2 - E_1}{kT}\right) = \frac{g_{D1}}{g_{D2}} \exp\left(\frac{\hbar\nu_{12}}{kT}\right) \quad (2.4)$$

Where, g_{D1} and g_{D2} are the degeneracies of the levels (similar to density of states N_C and N_V) and indicate the number of sub energy levels within E_1 and E_2 .

We then define τ_{21} as the lifetime of carriers in the conduction band before spontaneous emission takes place, with $A_{21} = \tau_{21}^{-1}$ being the Einstein coefficient for spontaneous emission. Under thermal equilibrium,

$$B_{12} = \left(\frac{g_{D2}}{g_{D1}} \right) B_{21} \quad (2.5)$$

$$\frac{A_{21}}{B_{21}} = \frac{8\pi V^3 n_r^3}{c^3} = \frac{\hbar\omega^3}{\pi^2 c^2} \quad (2.6)$$

Where, Eqn. (2.5) and Eqn. (2.6) are known as the Einstein Relations. If the degeneracy's are equal, then $B_{12}=B_{21}$. Examining Eqn. (2.4), we note that in order for sustained stimulation emission to occur; N_2 must be greater than N_1 . Otherwise, the energized electrons with which incoming photons resonate will be depleted from the conduction band. $N_2 > N_1$ defines population inversion, and if we assume that $\tau_r = \tau_{21}$, then $A_{21} = \tau_r^{-1}$ and

$$B_{21} = \frac{c^3}{8\pi V^3 n_r^3 \tau_r} = \frac{\lambda^3}{8\pi \tau_r} \quad (2.7)$$

2.5.6 Gain, Losses and the Lasing Condition

Population inversion enables lasing action and optical gain in a semiconductor, and this population inversion is achieved by creating nonequilibrium populations of the carriers in the bands. These nonequilibrium populations result from minority carriers injected across a forward-biased junction. In a lasing medium, stimulated downward transitions Eqn.(2.3) represent gain, and stimulated upward transitions Eqn.(2.1) represent loss. The luminescence from a semiconductor represents its spontaneous emission spectrum, which has a definite width [6]. For lasing to occur, the gain must be greater than or equal to the loss at a photon energy within this spectrum (generally the peak wavelength). Because the laser is built in a resonant cavity, a significant photon density arises in a supported cavity mode. This spontaneous emission induces stimulated emission, and emitted photons stimulate even further recombination in a chain-reaction fashion. Since the photon density is highest at the peak energy, they stimulate the most transitions; this means that the output spectrum grows and narrows simultaneously. This is the onset of super radiance. Thus the two conditions for lasing are: First the gain must be at least equal to the losses in the medium. Second the radiation must be coherent. The directionality and coherence of emitted light is maintained by constructing the laser in a Fabry-Perot cavity waveguide. The electric and magnetic fields that dictate waveguide modes operate according to the following wave equations (derived from Maxwell's equations) [5]

$$\Delta^2 E + \omega^2 \mu \epsilon_0 \epsilon_r E = 0 \quad (2.8)$$

$$\Delta^2 H + \omega^2 \mu \epsilon_0 \epsilon_r H = 0 \quad (2.9)$$

For the light to be guided through the desired area of the material (i.e., the active regions), it is necessary to confine the waveguide modes using cladding layers. The waveguide design determines how the light will be guided, and the cladding layers determine how it will be confined. The confinement factor Γ is the percentage of guided light that “fits” within the active layer. We can then define a modal gain which is equal to the threshold gain g_{th} multiplied by the confinement factor Γ . This modal gain is a measure of the power transferred from the active region into the propagating mode [6].

$$\Gamma \cdot g_{th} = \alpha_i + \frac{1}{2L} \ln \left(\frac{1}{R_1 R_2} \right) = \alpha_i + \alpha_m \quad (2.10)$$

Where, α_i is the internal loss in the medium, and α_m is the loss due to the mirrors or facets (with reflectivities R_1 and R_2) that define the cavity length L . The gain is amplified since the light being reflected between these two facets is in a gain medium. Eqn. (2.10) defines the threshold condition for lasing. The value of concentration which Eqn. (2.10) is true is the threshold carrier concentration n_{th} .

$$n_{th} = \frac{d_m}{d} \left(\frac{8\pi v_0^2 g_{th} \tau_r \Delta v n_r^2}{c^2} \right) \quad (2.11)$$

Where d_m is the thickness of the mode volume, and d is the thickness of the active layer, v_0 is the light velocity in a crystal, τ_r is the radiative carrier lifetime and n_r is the radiative carrier. We can then also define the population inversion necessary to satisfy the lasing condition,

$$N_{th} = \left(\frac{8\pi v_0^2 g_{th} \tau_r \Delta v n_r^2}{c^2} \right) \quad (2.12)$$

2.5.7 Operation of Laser

A laser consists of a gain medium inside an optical cavity, with a means to supply energy to the gain medium (as shown in Fig.2.6). The gain medium is a material (gas, liquid, or solid) with appropriate optical properties. In its simplest form, a cavity consists of two mirrors arranged such that light bounces back and forth, each time passing through the gain medium. Typically, one of the two mirrors, the output coupler, is partially transparent. All light that is emitted by the laser passes through this output coupler. Light of a specific wavelength that passes through the gain medium is amplified (increases in intensity); the surrounding mirrors ensure that most of the light makes many passes through the gain medium. Part of the light

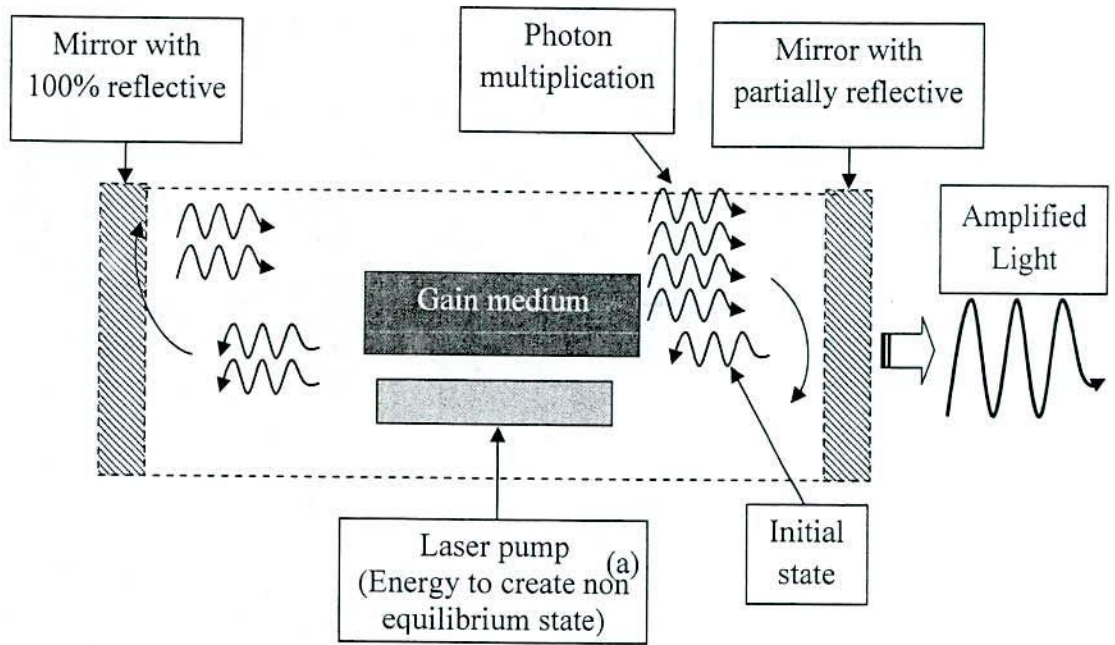


Fig.2.6. Key elements of the laser.

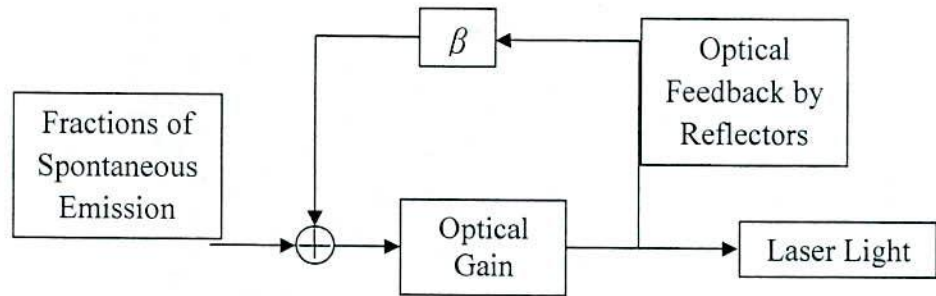


Fig.2.7. Equivalent circuit of Fig.2.6.

that is between the mirrors (i.e., is in the cavity) passes through the partially transparent mirror and appears as a beam of light. The process of supplying the energy required for the amplification is called pumping and is the energy is typically supplied as an electrical current or as light at a different wavelength.

2.6 References

- [1] K. Thyagarajan and Ajoy Ghatak, "Lasers: Fundamentals and Applications", Second Edition, Springer, New York, ISBN 978-1-4419-6442-7.
- [2] K.R Nambiar, "LASERS: Principles Type and Applications", New Age International Limited Publishers, New Delhi, ISBN 81-224-1492-3.
- [3] T. H. Maiman, "Stimulated Optical Radiation in Ruby", Nature, Vol. 187, No. 4736, pp. 493–494, 1960.
- [4] Takahiro Numai, "Fundamental of Semiconductor Lasers", Springer Series in Optical Sciences, ISBN0-387-40836-3, 2004.
- [5] Kamakhya Prasad Ghatak, Sitangshu Bhattacharya, Debashis, "Einstein Relation in Compound Semiconductors and Their Nanostructures", Springer Series in Materials Science, Vol. 116, ISBN 978-3-540-79556-8.
- [6] Bhattacharya, Pallab, "Semiconductor Optoelectronic Devices", 2nd Edition, (Prentice-Hall) 1997.

MODELING AND SIMULATION METHODOLOGY

3.1 Introduction

It is important for the better understanding of the physical device structure and analyze the methods to optimize the design parameters for InGaN lasers. This chapter describes the physical structure and mathematical models of the device. To analyze band structure profile one dimensional Schrödinger equations have been solved using **k.p** method with a 4×4 Luttinger-Kohn Hamiltonian matrix operator. Finite difference method has been employed for calculations. For laser characterization general laser equations are explained to simulate using computer programs. The thermal and equivalent circuit modeling are also discussed in this chapter.

3.2 Proposed Physical Model of Laser

The laser device comprising a hetero structure that is composed of an active layer and a pair of cladding layers which sandwiches the active layers in between. The optical guiding layers

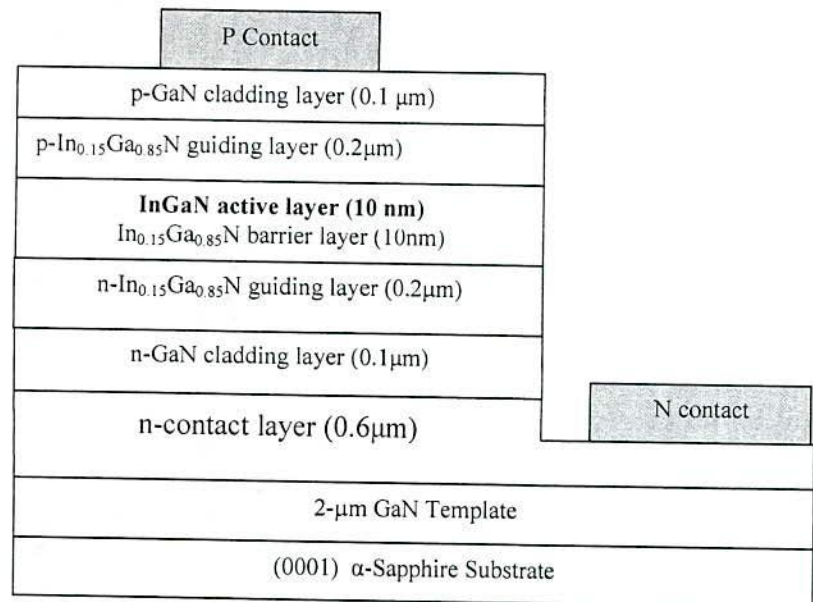


Fig.3.1. Schematic structure of the proposed edge emitting laser.

are positioned between one cladding layer and the active layer and between the active layer and the other cladding layer, a striped contact layer in which current injected into the laser device is confined. The schematic structure of the proposed 1.55- μm quantum-well heterostructure lasers using InGaN is shown in Fig.3.1. A c-plane sapphire wafer is used as the substrate. The laser structure consists of 0.6 μm -thick nickel as n-contact and gold as p-contact, 0.1 μm thick GaN cladding layer, 0.2 μm thick $\text{In}_{0.15}\text{Ga}_{0.85}\text{N}$ guiding layer, and a 10 nm thick InGaN active layer along with 10 nm thick $\text{In}_{0.15}\text{Ga}_{0.85}\text{N}$ barrier layer. The guiding layers termed as index guiding waveguides are used in laser to confine the laser light in active region. The cladding layers are used to reduce the penetration of the optical mode outside the guiding layers [1]. It facilitates to activate the leakage current due to drift and diffusion of electrons through the p-cladding layer. The leakage current increases as the cladding thickness is reduced [1-2].

3.3 Simulation Process

Simulation and characterization on InGaN based lasers are very immature. To realize a physical structure, simulations on structure and parameter optimization are necessary. This section describes the simulation processes adopted for analysis the proposed physical model.

3.3.1 Physical Properties

This section analyzes the physical model of the proposed laser structure. It includes band gap energy determination, composition of constituent materials, lattice constants and electronic band energy calculation for both conduction and valence bands.

3.3.1.1 Composition of In and Ga

In recent years most of the intensive research has been focused on Ga-rich $\text{In}_x\text{Ga}_{1-x}\text{N}$ and $\text{Ga}_x\text{Al}_{1-x}\text{N}$ alloys whose energy gaps cover the short wavelength visible and near ultraviolet parts of the electromagnetic spectrum [3-4]. It was suggested that the band gap of InN should be much smaller than 1.9 eV[5]. Recently new band gap of 0.65 eV for InN has been reported [5-6]. The band gap of the $\text{In}_x\text{Ga}_{1-x}\text{N}$ can be approximated by the parabolic form [7].

$$E_{g\text{InGaN}}(x) = xE_{g\text{InN}} + (1 - x)E_{g\text{GaN}} - bx(1 - x) \quad (3.1)$$

Here, $E_{g\text{InN}} = 0.69$ eV and $E_{g\text{GaN}} = 3.4$ eV, and Bowing parameter, $b=1.23$ eV (for $\text{In}_x\text{Ga}_{1-x}\text{N}$) [8-9]. Figure 3.2 shows the fraction of In and Ga in $\text{In}_x\text{Ga}_{1-x}\text{N}$.

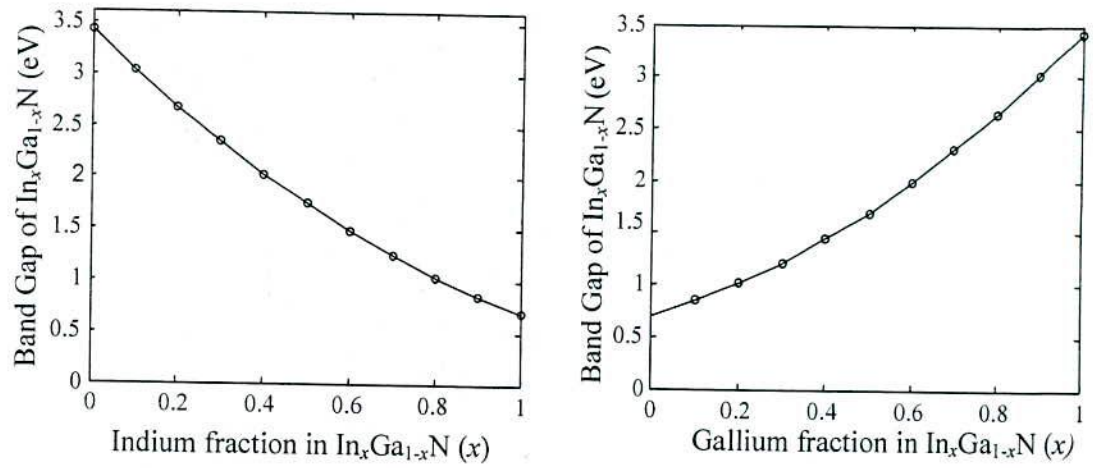


Fig.3.2. Composition of In and Ga in In_xGa_{1-x}N.

3.3.1.2 Lattice Constant

The chemical bonds of InGaN are predominantly covalent, which means that each atom is tetrahedrally bonded to four atoms of the other type. Because of the large difference in electro negativity of In and N atoms, there is a significant ionic contribution to the bond which determines the stability of the respective structural phase.

The lattice constants of the unstrained InGaN layer depend linearly on the indium composition. Lattice constants $a(x)$ and $c(x)$ of In_xGa_{1-x}N are predicted by Vegard's law as

$$a_{\text{InGaN}}(x) = (3.1986 + 0.3862x)\text{\AA} \quad (3.2)$$

$$c_{\text{InGaN}}(x) = (5.2262 - 0.574x)\text{\AA} \quad (3.3)$$

3.3.1.3 Refractive Index

In index guiding waveguides, a light is confined to a high refractive region and is surrounded

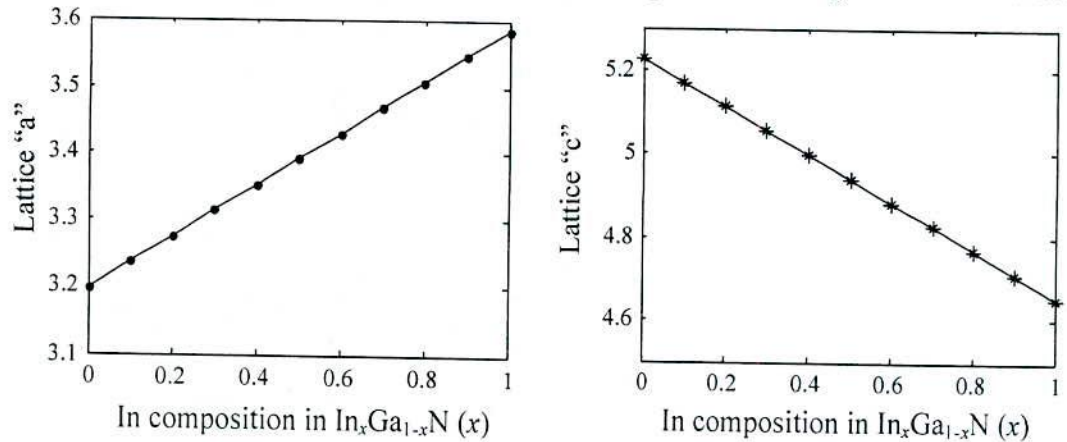


Fig.3.3.(a) Lattice constant $a(x)$ of In_xGa_{1-x}N. (b) Lattice constant $c(x)$ of In_xGa_{1-x}N.

by low refractive index region. If the refractive indexes n_a , n_g , and n_c represent the refractive indexes of active layer, guiding layer and cladding layer respectively and satisfy $n_a > n_g, n_c$, a light is confined to a region with n_a i.e. in the active layer. The gain guiding waveguides use a property that only a gain region amplifies a light, and a light seems to propagate in the gain region.

Optical reflection and wave guiding mainly depend on the refractive index profile inside the device and for photon energies close to the band gap, as the refractive index is a strong function of wavelength [10]. The refractive indexes of ternary alloys are extracted from GaN waveguide measurements using bandgap variations and are given by [7, 11]

$$n(\text{In}_x\text{Ga}_{1-x}\text{N}) = 2.5067 + 0.91x \quad (3.4)$$

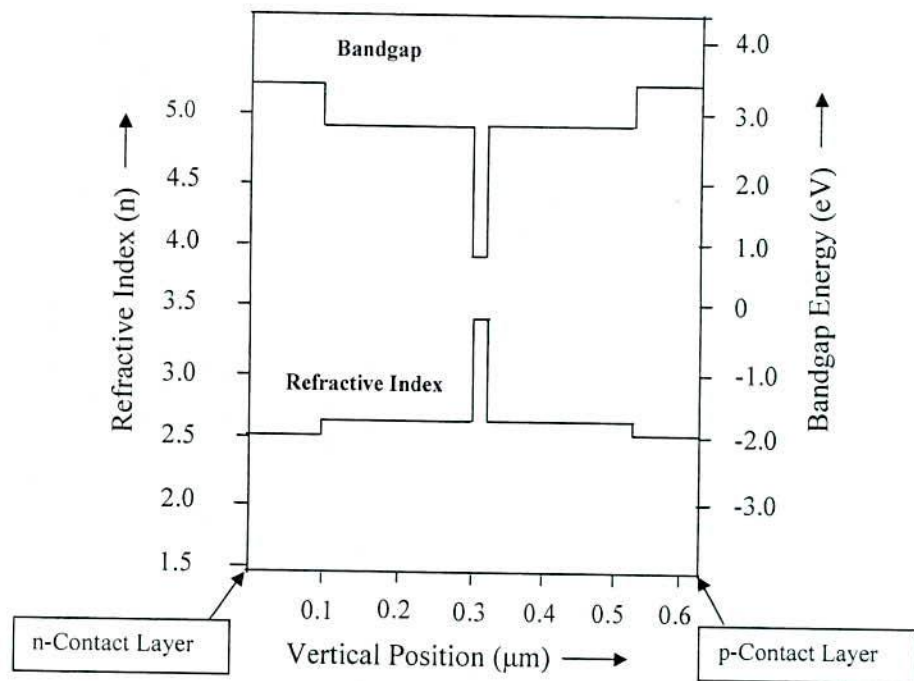


Fig. 3.4. Energy band diagram of InGaN quantum well together with refractive index profile.

Figure 3.4 shows the distributions of the energy and the refractive index of InGaN based quantum well laser. Under a forward bias, the holes are injected from the p cladding layer to the active layer, and the electrons are injected from the n-cladding layer to the active layer. The energy barrier for the holes is ΔE_v at the interface of the n-cladding layer and the active layer; that for the electrons is ΔE_c at the interface of the p-cladding layer and the active layer. In many semiconductors, their refractive indexes increase with a decrease in the band gap energies. Hence, the refractive index of the active layer n_a is usually greater than that of the p-

cladding layer n_p and that of the n-cladding layer n_n . As a result, a light is efficiently confined to the active layer, which results in a high light amplification rate. If n_a , n_c , and n_s be the refractive indexes of the guiding layer, the cladding layer and substrate respectively, then to confine a light in the guiding layer, we need $n_a > n_s \geq n_c$, and $n_f - n_s$ is usually in the order of 10^{-3} to 10^{-1} .

3.3.2 Electronic Energy Bands

The ternary nitride compounds AlGaN and InGaN can be grown both as hexagonal as well as in cubic structures [12-14]. Growth of Cubic InGaN quantum wells with high structural and optical quality has been reported by [15-17]. To make the calculation simple we assumed a cubic structure for our proposed InGaN based laser.

The time independent Schrödinger equation is given by [18-19]

$$E(k_t = 0)\psi_i = \left[-\frac{\hbar^2}{2m^*} \nabla^2 \psi_i + U_i \psi_i \right] \quad (3.5)$$

$$\text{Where, } \nabla^2 = \frac{\partial^2}{\partial x^2} + \frac{\partial^2}{\partial y^2} + \frac{\partial^2}{\partial z^2}$$

The Poisson's equation in the semiconductor is given by [18]

$$\nabla \cdot (\epsilon \nabla \Phi) = -\rho \quad (3.6)$$

Where, Φ is the electrostatic potential and ρ is the charge density given by

$$\rho = e(p - n + C_0) \quad \text{and} \quad C_0 = N_D^+ - N_A^-$$

Here, $e = 1.6 \times 10^{-19}$ C is the magnitude of a unit charge, p is the hole concentration, n is the electron concentration, N_D^+ is the ionized donor concentration, and N_A^- is the ionized acceptor concentration.

For one dimensional case (z-axis)

$$E\psi_i = \left[-\frac{\hbar^2}{2m^*} \frac{d^2}{dz^2} + U_i(z) \right] \psi_i(z) \quad (3.7)$$

If the energy dispersion relation for a single band n near k_0 , (assuming 0) is given by [18]

$$E_n(k) = E_n(0) + \sum_{\alpha, \beta} \frac{\hbar^2}{2} \left(\frac{1}{m^*} \right)_{\alpha\beta} k_\alpha k_\beta \quad (3.8)$$

For the Hamiltonian H , with a periodic potential $U(z)$ H_{op} is given by [18]

$$H_{op} \equiv \frac{\hbar^2}{2m} \frac{d^2}{dz^2} + U(z) \quad (3.9)$$

In this section, we study the calculation of the band structures of semiconductor quantum wells. Here we focus on the $\mathbf{k.p}$ method of the Luttinger-Kohn Hamiltonian.

3.3.2.1 Conduction Band

In the InGaN quantum well, the conduction bands are assumed to be parabolic. The effective mass theory for the conduction band is obtained from the dispersion relation [18]

$$E(k) = \frac{\hbar^2 k^2}{2m^*} \quad (3.10)$$

Where, the effective-mass of the electron in the conduction band is $m^* = m_b^*$ in the barrier region and $m^* = m_w^*$ in the quantum well. In the presence of the quantum-well potential,

$$V(z) = \begin{cases} V_0 (= \Delta E_c) & |z| > \frac{L_w}{2} \\ 0 & |z| \leq \frac{L_w}{2} \end{cases}$$

Where, the energies are all measured from the conduction band edge. For one dimensional case the time independent Schrödinger equation is given by [18]

$$E\psi_i = \left[-\frac{\hbar^2}{2m_e} \frac{d^2}{dz^2} + U_i(z) \right] \psi_i(z) \equiv [H_{op}]\{\Psi\} \quad (3.11)$$

In this case the Hamiltonian operator is

$$H_{op} = \left[-\frac{\hbar^2}{2m_e} \frac{d^2}{dz^2} + U_i(z) \right]$$

In finite difference [19] technique,

$$\left(\frac{\partial^2 \Psi^2}{\partial z^2} \right)_{z=z_n} \rightarrow \frac{1}{a^2} [\Psi_{i+1}(z) - 2\Psi_i(z) + \Psi_{i-1}(z)] \text{ and } U(z)\Psi(z) \rightarrow U(z_n)\Psi(z_n)$$

Let, $t_0 = \frac{\hbar^2}{2m_e a^2}$. This allows us to write,

$$\begin{aligned} & \left[-\frac{\hbar^2}{2m_e} \frac{d^2}{dz^2} + U_i(z) \right] \Psi_i(z) \\ &= -\frac{\hbar^2}{2m_e a^2} [\Psi_{i+1}(z) - 2\Psi_i(z) + \Psi_{i-1}(z)] + U_i(z)\Psi_i(z) \\ &= (U_i(z) + 2t_0)\Psi_i(z) - t_0\Psi_{i-1}(z) - t_0\Psi_{i+1}(z) \end{aligned}$$

So a 4x4 Hamiltonian matrix becomes

$$H = \begin{bmatrix} 2t_0 + U_1 & -t_0 & 0 & 0 \\ -t_0 & 2t_0 + U_2 & -t_0 & 0 \\ 0 & t_0 & 2t_0 + U_3 & -t_0 \\ 0 & 0 & -t_0 & 2t_0 + U_4 \end{bmatrix}$$

Now, the time independent Schrödinger equation becomes,

$$E \begin{Bmatrix} \Psi_1 \\ \Psi_2 \\ \Psi_3 \\ \vdots \\ \Psi_{N-1} \\ \Psi_N \end{Bmatrix} = \begin{bmatrix} 2t_0 + U_1 & -t_0 & 0 & 0 & \cdot & 0 \\ -t_0 & 2t_0 + U_2 & -t_0 & 0 & \cdot & 0 \\ 0 & -t_0 & 2t_0 + U_3 & -t_0 & \cdot & 0 \\ \cdot & \cdot & \cdot & \cdot & \cdot & \cdot \\ 0 & 0 & \cdot & \cdot & 2t_0 + U_{N-1} & -t_0 \\ 0 & 0 & 0 & 0 & -t_0 & 2t_0 + U_N \end{bmatrix} \begin{Bmatrix} \Psi_1 \\ \Psi_2 \\ \Psi_3 \\ \vdots \\ \Psi_{N-1} \\ \Psi_N \end{Bmatrix}$$

The eigen-values and eigen-vectors of the Hamiltonian matrix give the corresponding conduction band energies and corresponding wave vectors [19] i.e. $[V,D]=\text{eig}(H)$. Now the electron density in the conduction band is calculated from the wave functions Ψ as the square of the wave function, Ψ^2 , represents electron density at any given point. Since the square of any real number is zero or positive, it is clear that electron density cannot be negative, as expected intuitively.

3.3.2.2 Valence Band

In the InGaN quantum well the valence bands are assumed to be non parabolic. For a given quantum-well potential,

$$V_h(z) = \begin{cases} 0 & |z| \leq \frac{L_w}{2} \\ -\Delta E_c & |z| > \frac{L_w}{2} \end{cases}$$

The Luttinger-Kohn Hamiltonian matrix in the dependency on wave function is defined as [20-21]

$$H^{LK} = \begin{bmatrix} P+Q & -S & R & 0 \\ -S^* & P-Q & 0 & R \\ R^* & 0 & P-Q & S \\ 0 & R^* & S^* & P+Q \end{bmatrix}$$

Where, the values of P, Q, R and S are given by [21-23]

$$P = \frac{\hbar^2 \gamma_1}{2m_0} (k_t^2 + k_1^2 + \frac{\partial^2}{\partial z^2}), Q = \frac{\hbar^2 \gamma_2}{2m_0} (k_t^2 + k_1^2 - 2 \frac{\partial^2}{\partial z^2})$$

$$R = \frac{\sqrt{3}\hbar^2}{2m_0} [-\gamma_2(k_t^2 - k_2^2) + 2i\gamma_3 k_1 k_2] \text{ and } S = \frac{\hbar^2 \gamma_3}{m_0} \sqrt{3}(k_t - ik_2) \frac{\partial}{\partial z}$$

Now,

$$P+Q = \frac{\hbar^2}{2m_0} [(\gamma_1 + \gamma_2)k_t^2 - (\gamma_1 - 2\gamma_2) \frac{\partial^2}{\partial z^2}]$$

$$P-Q = \frac{\hbar^2}{2m_0} [(\gamma_1 - \gamma_2)k_t^2 - (\gamma_1 + 2\gamma_2) \frac{\partial^2}{\partial z^2}] \text{ and } S = \frac{\hbar^2 \gamma_3}{m_0} \sqrt{3}(k_t - ik_2) \frac{\partial}{\partial z}$$

For Luttinger-Kohn Hamiltonian matrix $E\Psi_{hi} = H\Psi_{hi}(z)$

Taking, $t_0 = \frac{\hbar^2}{2m_e a^2}$ and using finite difference method [18], we get

$$(P+Q)\Psi_{j,n}(z) = \left\{ \frac{\hbar^2}{2m_0} [(\gamma_1 + \gamma_2)k_t^2 - (\gamma_1 - 2\gamma_2) \frac{\partial^2}{\partial z^2}] + U_i(z) \right\} \Psi_{j,n}(z)$$

$$\begin{aligned}
&= \left\{ \frac{\hbar^2}{2m_0} \left[(\gamma_1 + \gamma_2) k_t^2 - (\gamma_1 - 2\gamma_2) \frac{(-2)}{a^2} \right] + U_i(z_i) \right\} \Psi_{j,n}(z_i) + \\
&\left\{ \frac{\hbar^2}{2m_0} \left[(\gamma_1 + \gamma_2) k_t^2 - (\gamma_1 - 2\gamma_2) \frac{1}{a^2} \right] + U_{i+1}(z_{i+1}) \right\} \Psi_{j,n}(z_{i+1}) + \\
&\left\{ \frac{\hbar^2}{2m_0} \left[(\gamma_1 + \gamma_2) k_t^2 - (\gamma_1 - 2\gamma_2) \frac{1}{a^2} \right] + U_{i-1}(z_{i-1}) \right\} \Psi_{j,n}(z_{i-1}) \\
&= A_i \Psi_{j,n}(z_i) + B_i \Psi_{j,n}(z_{i+1}) + B_i \Psi_{j,n}(z_{i-1})
\end{aligned} \tag{3.12}$$

Where, $A_i = \frac{\hbar^2}{2m_0} \left[(\gamma_1 + \gamma_2) k_t^2 - (\gamma_1 - 2\gamma_2) \frac{(-2)}{a^2} \right] + U_i(z_i)$

$$B_i = \frac{\hbar^2}{2m_0} \left[(\gamma_1 + \gamma_2) k_t^2 - (\gamma_1 - 2\gamma_2) \frac{1}{a^2} \right] + U_{i-1}(z_{i-1})$$

Similarly, $(P - Q) \Psi_{j,n}(z) = A_i \Psi_{j,n}(z_i) + B_i \Psi_{j,n}(z_{i+1}) + B_i \Psi_{j,n}(z_{i-1})$

$$(-S) \Psi_{j,n}(z) = -\frac{\sqrt{3}\hbar^2\gamma_3}{m_0} (k_t - ik_2) \frac{\partial}{\partial z} \Psi_{j,n}(z)$$

$$= -\frac{\sqrt{3}\hbar^2\gamma_3}{m_0} (k_t - ik_2) \frac{\Psi_{j,n}(z_{i+1}) + \Psi_{j,n}(z_{i-1})}{2a}$$

$$= C_i \Psi_{j,n}(z_{i+1}) + C_i \Psi_{j,n}(z_{i-1}) \tag{3.13}$$

Where, $C_i = -\frac{\sqrt{3}\hbar^2\gamma_3}{m_0} (k_t - ik_2) \frac{1}{2a}$

$$R \Psi_{j,n}(z_i) = \frac{\sqrt{3}\hbar^2}{2m_0} \left[-\gamma_2 (k_t^2 - k_2^2) + 2i\gamma_3 k_1 k_2 \right] \Psi_{j,n}(z_i)$$

Now the Hamiltonian matrix for 3 nodes is shown as

$$H^{LK} = \begin{pmatrix}
A_1 & 0 & E_1 & 0 & B_2 & -D_2 & 0 & 0 & 0 & 0 & 0 & 0 \\
0 & A_1^* & 0 & E_1 & -D_2^* & B_2^* & 0 & 0 & 0 & 0 & 0 & 0 \\
E_1 & 0 & A_1^* & 0 & 0 & 0 & B_2^* & D_2 & 0 & 0 & 0 & 0 \\
0 & E_1^* & 0 & A_1 & 0 & 0 & D_2^* & B_2 & 0 & 0 & 0 & 0 \\
B_1 & -C_1 & 0 & 0 & A_2 & 0 & E_2 & 0 & B_3 & -C_3 & 0 & 0 \\
-C_1^* & B_1^* & 0 & 0 & 0 & A_2^* & 0 & E_2 & -C_3^* & B_3^* & 0 & 0 \\
0 & 0 & B_1^* & C_1 & E_2^* & 0 & A_2^* & 0 & 0 & 0 & B_3^* & C_3 \\
0 & 0 & C_1^* & B_1 & 0 & E_2^* & 0 & A_2 & 0 & 0 & C_3^* & B_3 \\
0 & 0 & 0 & 0 & B_2 & -C_2 & 0 & 0 & A_3 & 0 & E_3 & 0 \\
0 & 0 & 0 & 0 & -C_2^* & B_2^* & 0 & 0 & 0 & A_3^* & 0 & E_3 \\
0 & 0 & 0 & 0 & 0 & 0 & B_2^* & C_2 & E_3^* & 0 & A_3^* & 0 \\
0 & 0 & 0 & 0 & 0 & 0 & C_2^* & B_2 & 0 & E_3^* & 0 & A_3
\end{pmatrix}$$

3.3.3 The fundamental Set of Equations

The general set of equations used for parameter optimization and performance evaluation has been discussed in this section. This includes gain of the laser, threshold behavior, temperature dependency of gain and threshold current, efficiency and output power.

3.3.3.1 Gain

This section describes different types of gain. Optical gain, material gain, modal gain and optical power gain of 1.55 μm InGaN based lasers has been presented.

i. Optical gain

The photon current associated with an electromagnetic wave travelling through a semiconductor is described by [10]

$$I_{\text{ph}} = I_{\text{ph}}^0 \exp(-\alpha x) \quad (3.14)$$

Where, α is the absorption coefficient. If electrons are pumped in the conduction band and holes in the valance band, the electron- hole recombination process (photon emission) can be stronger thnn the reverse process of electron- hole generation (photon absorption). In general, the gain coefficient is defined by, gain = emission coefficient – absorption coefficient.

If $f^e(E^e)$ and $f^h(E^h)$ denote the electron and hole occupation, the emission coefficient depends upon the product of $f^e(E^e)$ and $f^h(E^h)$ while the absorption coefficient depends upon the product of $(1 - f^e(E^e))$ and $(1 - f^h(E^h))$. For this transitions we have

$$n = \frac{N_c \exp(E_{\text{Fc}} - E_c)}{KT} \quad (3.15)$$

$$p = \frac{N_v \exp(E_{\text{Fv}} - E_v)}{KT} \quad (3.16)$$

$$\text{Where, } N_c = 2 \left(\frac{2\pi m_e^* KT}{h^2} \right)^{3/2} \text{ and } N_v = 2 \left(\frac{2\pi m_h^* KT}{h^2} \right)^{3/2}$$

Here, n and p are the electron concentration and hole concentration respectively; E_c and E_v are the energy of the bottom of the conduction band and that of the top of the valance band, respectively; $K=1.3807 \times 10^{-23} \text{ J K}^{-1}$ is Boltzman constant; $T=300\text{K}$ is an absolute temperature; N_c and N_v are the effective density of states for the electrons and holes, respectively; m_e^* and m_h^* are the effective mass of the electrons and holes, respectively; and $h= 6.6 \times 10^{-34} \text{ Js}$ is Planck's constant. The energies E^e and E^h are given by [10]

$$E^e = E_c + (\hbar\omega - E_g) \frac{m_h^*}{m_e^* + m_h^*} \quad (3.17)$$

$$E^h = E_v - (\hbar\omega - E_g) \frac{m_e^*}{m_e^* + m_h^*} \quad (3.18)$$

The occupation probabilities are

$$f^e(E^e) = \frac{1}{\left[\exp\left(\frac{E^e - E_{Fc}}{KT}\right) + 1\right]} \quad (3.19)$$

$$f^h(E^h) = \frac{1}{\left[\exp\left(\frac{E_{Fv} - E^h}{KT}\right) + 1\right]} \quad (3.20)$$

The quasi Fermi levels are [10]

$$E_{Fc} = E_c + KT \left[\ln\left(\frac{n}{N_c}\right) + \frac{\left(\frac{n}{N_c}\right)}{\sqrt{8}} \right] \quad (3.21)$$

$$E_{Fv} = E_v - KT \left[\ln\left(\frac{p}{N_v}\right) + \frac{\left(\frac{p}{N_v}\right)}{\sqrt{8}} \right] \quad (3.22)$$

Gain is approximately given by [10]

$$G(\hbar\omega) = 5.7 * \frac{10^4 (\hbar\omega - E_g)^{\frac{1}{2}} [f^e(E^e) + f^h(E^h) - 1]}{\hbar\omega} \text{ cm}^{-1} \quad (3.23)$$

ii. Material Gain

The material gain can be determined from the spontaneous emission rate using [24]

$$G(N_w) = g_0 \left(\frac{N_w}{V_w} - N_{w0} \right)^\zeta \quad (3.24)$$

Where, N_w is the number of quantum well, v_w is the volume of quantum well, N_{w0} is the initial carrier concentration in the well and ζ is a factor. A narrow well has a larger separation of sub bands, resulting in sharper gain and spontaneous emission spectra than those of a wider well. It is clearly seen that the TM polarized gain is very small, as expected from the valence sub band structures, since the HH and LH sub bands contribute mostly to TE polarization.

iii. Modal Gain

Γ_g , the modal gain, does not depend explicitly on w , the quantum well width. It depends only indirectly on w in that changing the width affects the separation between the sub bands which influences the positioning of the quasi-Fermi level; the overlap between electrons and holes is also affected [25]

$$\Gamma_g = \frac{1}{L} \ln \frac{1}{R_m} + \alpha \quad (3.25)$$

Here, g is the material gain, L is the cavity length, R_m is the mirror reflectivity, and α is the non radiative absorption loss per unit length.

iv. Optical power gain

The optical power gain coefficient of laser is written as [10]

$$g = \frac{1}{L} \ln \frac{1}{\sqrt{R_1 R_2}} \quad (3.26)$$

Where the right hand side is called the mirror loss and R_1 and R_2 denotes the reflectivity's of the mirrors.

3.3.3.2 Efficiency

External quantum efficiency and power conversion efficiency for InGaN based lasers are described in this section.

i. External Quantum Efficiency

The external differential quantum efficiency η_d (in no units) is defined as the number of photons emitted outward per injected carrier. The external differential quantum efficiency, η_d for the total light output is given by [10]

$$\eta_d = \frac{\frac{\Delta P}{\hbar \omega}}{\left(\frac{\Delta I}{e}\right)} = \frac{\Delta P}{\Delta I} \frac{e}{\hbar \omega} \quad (3.27)$$

Where, ω is an angular frequency of the light, \hbar is Dirac's constant, and q is the elementary charge. The total loss is a sum of the internal loss and the mirror loss. For a reference system placed outside the optical cavity, the mirror loss indicates the light emission rate from the optical cavity. As a result, using the internal quantum efficiency η_i , which is defined as the number of photons emitted inside the optical cavity per injected carrier, the external differential quantum efficiency η_d is expressed as

$$\eta_d = \eta_i \frac{(\text{Mirror Loss})}{(\text{Total Loss})} = \eta_i \frac{\frac{1}{2L} \ln \frac{1}{R_1 R_2}}{\alpha_i + \frac{1}{2L} \ln \frac{1}{R_1 R_2}} = \eta_i \frac{\ln \frac{1}{R_1 R_2}}{2\alpha_i L + \ln \frac{1}{R_1 R_2}} \quad (3.28)$$

Where, the optical losses at the facets due to the absorption or the scattering were assumed to be negligible. If waveguide loss α_w and the unavoidable signal shot noise loss α_u are considered then

$$\eta_d = \eta_i \frac{(\text{Mirror Loss})}{(\text{Total Loss})} = \eta_i \frac{\frac{1}{2L} \ln \frac{1}{R_1 R_2}}{\alpha_i + \alpha_w + \alpha_u + \frac{1}{2L} \ln \frac{1}{R_1 R_2}} \quad (3.29)$$

Where, α_w indicates the internal waveguide loss and α_u indicates the unavoidable signal shot noise loss which is not more than 5 % of the total loss [26].

ii. Power Conversion Efficiency

The power conversion efficiency is calculated as below [27], where η_d is the differential quantum efficiency and V_b is the bias voltage.

$$\eta_P = \eta_d \frac{E_g}{V_b} \left(1 - \frac{I_{th}}{I}\right) \quad (3.30)$$

3.3.3.3 I-V Characteristics

This section describes the electrical characteristics of the proposed laser structure. The electrical characteristics include current –voltage relationship, determination of threshold current density, temperature dependency.

i. I-V relationship

If we assume that the electron concentration n is equal to the hole concentration p , we can write the rate equations for the carrier concentration n and the photon density S of the laser light as[10]

$$\frac{dn}{dt} = \frac{I}{ed} - G(n)S - \frac{n}{\tau_n} \quad (3.31)$$

$$\frac{ds}{dt} = G(n)S - \frac{S}{\tau_{ph}} + \beta_{sp} \frac{n}{\tau_r} \quad (3.32)$$

In a steady state, Eqn. (3.31) and Eqn. (3.32) reduces to,

$$S = -\beta_{sp} \frac{n}{\tau_r} \frac{1}{G(n) - \frac{1}{\tau_{ph}}} \quad (3.33)$$

$$I = eV_a \left[G(n)S + \frac{n}{\tau_n} \right] \quad (3.34)$$

Here, I is the injection current and $V_a = S_A d$ is the volume of the active layer in which S_A is the area of the active layer, d is the active layer thickness, β_{sp} is the spontaneous emission coupling factor, τ_{ph} is the photon lifetime and τ_r is the radiative recombination lifetime. A flowing current in semiconductor lasers consists of the diffusion current, the drift current, and the recombination current. Here, it is assumed that the radiative recombination is dominant, and the diffusion and drift currents are neglected, as shown in Eqn. (3.32).

The carrier concentration n is approximately given by

$$n = n_i \exp\left(\frac{eV}{2k_B T}\right) \quad (3.35)$$

Where, V is a voltage across the p-n-junction and n_i is the intrinsic carrier concentration, which is expressed as

$$n_i = 2 \left(\frac{2\pi k_B T}{h^2}\right)^{\frac{3}{2}} (m_e m_h)^{\frac{3}{4}} \exp\left(\frac{-E_g}{2k_B T}\right) \quad (3.36)$$

Here, k_B is Boltzmann's constant, T is an absolute temperature, h is Planck's constant, m_e and m_h are the effective masses of the electron and the hole, respectively, and E_g is the band gap energy of the active layer.

From Eqn. (3.33)–(3.36), a relation between the injection current I and the voltage V is given by

$$I = eV_a \left[-\beta_{sp} \frac{n_i e^{eV/2k_B T}}{\tau_r} \frac{G(n_i e^{eV/2k_B T})}{G(n_i e^{eV/2k_B T}) - \tau_p - 1} + \frac{n_i e^{eV/2k_B T}}{\tau_n} \right] \quad (3.37)$$

ii. Threshold Current Density

Threshold current density is the key element to improve the device performance. To calculate the threshold current density, first, we consider the rate equations below the threshold, where net stimulated emission is negligible and $S = 0$.

$$\text{Therefore, } \frac{dn}{dt} = \frac{J}{ed} - \frac{n}{\tau} \quad (3.38)$$

In a steady state ($d/dt = 0$), from Eqn. (3.38), the carrier concentration n is given by

$$n = \frac{J}{ed} \tau_n \quad (3.39)$$

$$\text{Thus, } J = \frac{ed}{\tau_n} n$$

When the carrier concentration n increases from 0 to the threshold carrier concentration n_{th} , we expect that Eqn. (3.39) is still satisfied at the threshold. As a result, the threshold current density J_{th} is expressed as

$$J_{th} = \frac{ed}{\tau_n} n_{th} \quad (3.40)$$

From Eqn. (3.40), it is found that a small n_{th} and a long τ_n lead to a low J_{th} . Because the optical confinement factor Γ_a of the active layer depends on the active layer thickness d , the threshold current density n_{th} is a function of d and there exists an optimum d value to achieve the lowest J_{th} . Again, we calculate the threshold carrier concentration n_{th} using the rate

equations above the threshold. In usual semiconductor lasers, the spontaneous emission coupling factor β_{sp} is on the order of 10^{-5} . Therefore, as the first approximation, we neglect the term $\beta_{sp}n/\tau_r$.

At the threshold, the threshold carrier concentration n_{th} is written as

$$n_{th} = n_0 + \frac{1}{(g_0\tau_{ph}\Gamma_a)} \quad (3.41)$$

In semiconductor lasers, changes in the cavity length, the facet reflectivity's, and the refractive indexes during laser operation are small. Therefore, above the threshold, the carrier concentration n is clamped on the threshold carrier concentration n_{th} . The threshold current density J_{th} becomes

$$J_{th} = \frac{ed}{\tau_n} \left(n_0 + \frac{1}{g_0\tau_{ph}\Gamma_a} \right) \quad (3.42)$$

Here, it is clearly shown that the threshold current density J_{th} depends on the optical confinement factor Γ_a . The threshold current tends to increase with temperature, the temperature dependence of the threshold current density J_{th} being approximately exponential for most common structures. Dependence of the threshold current density on temperature is empirically expressed as

$$J_{th} = J_0 \exp\left(\frac{T_j}{T_0}\right) \quad (3.43)$$

Where, J_0 is a coefficient, T_j is the temperature in active layer and T_0 is the characteristic temperature, which indicates dependency of the threshold current density with the temperature.

3.3.3.4 Optical Characteristics

The optical characteristics include optical output power variations with input current, optical confinement factor. These terms are presented in this section.

i. Output Power

We assume that the nonradiative recombination is negligible, which lead to $\tau_r \approx \tau_n$. In steady state, when the coupling of the spontaneous emission to the lasing mode reduced to [10]

$$\frac{J}{ed} = \Gamma_a g_0 (n - n_0) S + \frac{n}{\tau_n} \quad (3.44)$$

$$\frac{S}{\tau_{ph}} = \Gamma_a g_0 (n - n_0) S + \beta_{sp} \frac{n}{\tau_n} \quad (3.45)$$

Therefore the carrier concentration n and the photon density S are given by

$$n = \frac{nth(X - \sqrt{X^2 - Y})}{2(1 - \beta_{sp})} \quad (3.46)$$

Where,

$$X = 1 + \frac{J}{J_{th}} - \beta_{sp} \frac{n_0}{n_{th}} \quad \text{and} \quad Y = 4(1 - \beta_{sp}) \frac{J}{J_{th}}$$

The current for which the gain satisfies the lasing condition is the threshold current of the laser, I_{th} . Below the threshold current very little light is emitted by the laser structure. For an applied current larger than the threshold current, the output power, P_{out} , increases linearly with the applied current. The output power therefore equals

$$P_{out} = \frac{h\omega}{e} (I - I_{th}) \quad (3.47)$$

Where, $h\omega$ is the energy per photon. The factor, $h\omega$, indicates that only a fraction of the generated photons contribute to the output power of the laser as photons are partially lost through the other mirror and throughout the waveguide.

ii. Optical Confinement Factor

Optical confinement factor is the ratio of the intensity of the light existing in the relevant layer to the total light intensity.

$$\Gamma^8 = 2\pi^2(n_a^2 - n_c^2) \left(\frac{d}{\lambda}\right)^2 \quad (3.48)$$

Where, $\Gamma = \frac{\Gamma^8}{1 + \Gamma^8}$, n_a = Refractive index of the active layer, n_c = Refractive index of cladding layer and d is the active layer thickness.

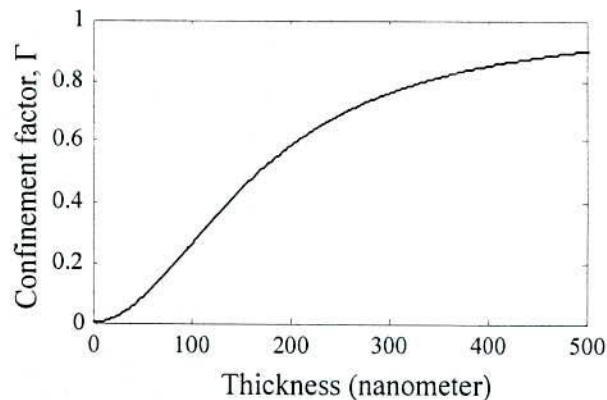


Fig.3.5. Active layer thickness vs. optical confinement factor.



Figure 3.5 shows that the optical confinement factor varies with active layer thickness. To design our device we choose active layer thickness as 10 nm and from figure optical confinement factor is 0.0035 corresponding to this thickness. The optical confinement factor Γ is an important parameter to design the optical losses or the optical gains in the optical waveguides.

3.4 Thermal Modeling of InGaN Based Laser

The thermal model is a representation of the thermally dependent threshold current and output power. By introducing a thermally dependent empirical offset current (I_{off}) into the rate equations, we are able to model the temperature-dependent threshold current and output power roll-over at different ambient temperatures. This accounts for all the static thermal effects like thermal leakage of carriers out of the active region, heat diffusion. For the quantum well structure (Fig.3.1) after the addition of the offset current, the modified rate equations in quantum well laser can be expressed as [28-29]

$$\frac{dN(t)}{dt} = \frac{[I(t) - I_{off}(T)]}{eV_a} - g_0 \frac{[N(t) - N_0]S(t)}{1 + \epsilon S(t)} - \frac{N(t)}{\tau_n} \quad (3.49)$$

$$\frac{dS(t)}{dt} = -\frac{S(t)}{\tau_p} + \frac{\beta_{sp}N(t)}{\tau_n} + \frac{g_0 [N(t) - N_0]S(t)}{1 + \epsilon S(t)} \quad (3.50)$$

Where, e is the electron charge, V_a is the volume of active region, g_0 is the gain slope, ϵ is the gain saturation parameter, τ_n is the carrier lifetime, Γ is the optical confinement factor, N_0 is the carrier density at transparency, τ_p is the photon lifetime, β_{sp} is the spontaneous emission coupling coefficient. The optical power is defined as [30]

$$P(t) = \frac{S(t)V_a h\nu}{2\Gamma\tau_p} \quad (3.51)$$

Output power is also defined as [31-32]

$$P_0 = \eta[I - I_{th0} - I_{off}(T_0 + (IV - P_0)R_{th})] \quad (3.52)$$

Where, $I_{off}(T) = a_0 + a_1T + a_2T^2 + a_3T^3 + a_4T^4 + \dots$

and $V = IR_s + V_T \ln\left(1 + \frac{I}{I_s}\right)$, $T = T_0 + (IV - P_0)R_{th} - \tau_{th} \frac{dT}{dt}$

Under DC conditions $\frac{dT}{dt}$ is zero.

The thermal rate equation is written as [28]

$$C_{th} \frac{dT}{dt} = -\frac{\Delta T}{R_{th}} + P_j + P_{nR} \quad (3.53)$$

Where, R_{th} is the equivalent thermal resistor defined as

$$R_{th} = \frac{1}{\kappa} \left(\frac{L_{active}}{WL} + \frac{L_{sub}}{W_{sub}L} \right) \text{ and } C_{th} = LWN_w L_w \rho_m c_p$$

Where, L_{sub} and W_{sub} are the substrate thickness and width, respectively and L_{active} is the total active region thickness. This thermal resistance is important as the behavior of a laser diode is affected by an increase of temperature within its volume during operation, which is determined by the value of the thermal resistance of the device.

The rise of temperature mainly due to nonradiative recombination processes as well as absorption of the generated radiation and Joule heating. This temperature increase influences adversely on emission, reliability and the operating characteristics of the laser. The temperature rise in the active region of the laser due to current injection of magnitude I is calculated as

$$\Delta T = R_{th} U_0 I_{app} + R_{th} R_0 I_{app}^2 - R_{th} L \quad (3.54)$$

Where, I_{app} is the applied input current intensity, U_0 is the positive turn-on voltage of the corresponding ideal diode and R_s is the series resistance.

The dependence $\Delta T(t)$ has been analyzed using (analogically to electric circuits) equivalent thermal ladder $R_{Th}C_{Th}$ circuits of the Foster and Cauer types, where R_{Th} corresponds to the thermal resistance and C_{Th} is the heat capacity of elements of the internal device structure and external heat sink. The mathematical form of $\Delta T(t)$ dependence is most simple for the Foster circuit presentation [33], i.e.

$$\Delta T(t) = P_T \sum_i R_{Thi} \left(1 - \exp \left(-\frac{t}{\tau_i} \right) \right) \quad (3.55)$$

This thermal resistance R_{thi} is given by [34]

$$R_{thi} = \frac{\Delta T}{P_{heat}} = \frac{\Delta T}{(P_{el} - P_{opt})} \quad (3.56)$$

Here P_T is the power dissipated by the device, R_{Thi} is the thermal resistance of the i -th element, τ_i is the heat time constant for the i -th element of the source. The heat flux P_T is related to the electric power P_{el} according to the relation $P_T = (1-\eta)P$, where η is the power efficiency of the laser source. From Eqn. (3.56) we construct a special function $R_T^*(\tau^*)$, i.e.

$$R_T^*(\tau^*) = \sum_i R_{Thi} \frac{\tau_i^*}{\tau_i} \exp \left(1 - \frac{\tau^*}{\tau_i} \right) \quad (3.57)$$

Using this formula and the measured $\Delta T(t)$ dependence, values of R_{Thi} and τ_i can be obtained. The maxima of the function $R_T^*(\tau^*)$ give the thermal resistance values for the device elements R_{Thi} , as well as their positions τ^* on the time scale corresponding to the time constants $\tau_i = R_{Thi}C_{Thi}$.

3.5 Equivalent Circuit Modeling of InGaN Based Laser

For the development of optoelectronic device models which can be used in conjunction with electronic components, a study of equivalent circuit model of quantum well lasers has been carried out. Circuit-level simulation of InGaN based semiconductor lasers is presented in this section. Initially, the equivalent circuit is implemented from the rate-equation of the quantum-well laser. Then the PSPICE simulation is used to determine the output characteristics of the laser. This model determines the correct numerical solution of the rate equations during dc simulation. It also allows to calculate the light output-injection current (LI) characteristics, threshold behavior, and transit time effect.

i. Mathematical model

The rate equations for quantum well lasers are given by [28-29,35-36]

$$\frac{dN(t)}{dt} = \eta_i \frac{I(t)}{eV_a} - \frac{N(t)}{\tau_n} - g_0 \frac{N(t)S(t)}{1+\epsilon S(t)} \quad (3.58)$$

$$\frac{dS(t)}{dt} = -\frac{S(t)}{\tau_p} + \frac{\beta N(t)}{\tau_n} \Gamma_c + \frac{g_0 N(t)S(t)}{1+\epsilon S(t)} \Gamma_c \quad (3.59)$$

$$\frac{S}{P_f} = \frac{\lambda \tau_p}{\eta_c V_a h c} = \vartheta \quad (3.60)$$

Where, N =equilibrium carrier concentration, I =injection current, $\frac{N(t)}{\tau_n}$ =the carrier recombination rate= $AN+BN^2+CN^3$, where A , B , and C are the unimolecular, radiative, and Auger recombination coefficients, respectively, S = photon density= S_{tot}/V_a , where, S_{tot} is again the total number of photons in the active volume, $\beta=\beta_A AN+\beta_B BN^2+\beta_C CN^3$, where β_A , β_B , and β_C are coupling coefficients, P_f = the output power, V_a = is the volume of a single QW, η_i =is the current-injection efficiency, Γ_c =is the optical confinement factor of one QW, g_0 =is the carrier dependent gain coefficient, τ_p =is the photon lifetime, λ =is the lasing wavelength, η_c = is the output-power coupling coefficient, $\frac{1}{1+\epsilon S(t)}$ = the gain saturation term.

ii. Model Implementation

To convert the rate equations into circuit model, multiplying Eqn. (3.58) by $\frac{eV_a}{\eta_i}$ we get,

$$\frac{eV_a}{\eta_i} \frac{dN(t)}{dt} = I - \frac{eV_a}{\eta_i} \frac{N(t)}{\tau_n} - g_0 \frac{eV_a}{\eta_i} \frac{N(t)S(t)}{1+\epsilon S(t)} \quad (3.61)$$

$$I = \frac{1}{\eta_i} I_n + \frac{\tau_n}{\eta_i} \frac{dI_n}{dt} + g_0 \frac{eV_a}{\eta_i} \frac{N_e \exp\left(\frac{eV}{nkT}\right) S(t)}{1+\epsilon S(t)} \quad (3.62)$$

Where, $G_0 = eV_a g_0$, $I_n = \frac{eV_a N(t)}{\tau_n}$, $N = N_e \exp\left(\frac{eV}{nkT}\right)$

So,
$$\frac{dN(t)}{dt} = \frac{\tau_n}{eV_a} \frac{dI_n}{dt}$$

$$\therefore \frac{eV_a}{\eta_i} \frac{dN(t)}{dt} = \frac{\tau_n}{\eta_i} \frac{dI_n}{dt}$$

Current I of Eqn. (3.62) is equal to three related current components at quantum well regions i.e. I_n , $I_1 = \frac{\tau_n}{eV_a} \frac{dI_n}{dt}$ and the stimulated emission component I_2 . The p-n heterojunction voltage V_j can be represented by one ohmic resistance R_e , series-connected with Shockley p-n junction diode (shown in Fig.3.6). $C_d = C_0 \left(1 - \frac{V_j}{V_d}\right)^{-\frac{1}{2}}$, a junction depletion capacitance is added to the circuit, where C_0 is the zero bias depletion capacitance, V_j is the junction voltage, V_d is the build-in potential.

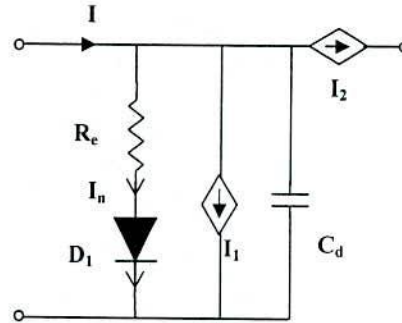


Fig.3.6. PSPICE circuit model of eqn. (3.62)

Now, multiplying Eqn. (3.59) by qV_a we get,

$$eV_a \frac{dS(t)}{dt} = -eV_a \frac{S(t)}{\tau_p} + eV_a \frac{\beta N(t)}{\tau_n} \Gamma_c + eV_a \frac{g_0 N(t) S(t)}{1 + \epsilon S(t)} \Gamma_c$$

$$C_p \frac{dS(t)}{dt} + \frac{S(t)}{R_p} = G_0 \frac{N(t) S(t)}{1 + \epsilon S(t)} \Gamma_c + \beta I_n \Gamma_c$$

$$\therefore \frac{S(t)}{\Gamma_c R_p} + \frac{C_p}{\Gamma_c} \frac{dS(t)}{dt} = G_0 \frac{N(t) S(t)}{1 + \epsilon S(t)} + \beta I_n \quad (3.63)$$

Where, $R_p = \frac{\tau_p}{C_p}$, $G_0 = D(J_{nom} - 2 \times 10^{13})^2$ [37]

Here, $D =$ a constant and $J_{nom} = \frac{I_n}{V_a}$.

In Eqn. (3.63), the first two terms represents a resistance (in parallel) and a capacitance. Again, the optical emission consists of a spontaneous component βI_n and a stimulated

component $G_0 \frac{N(t)S(t)}{1+\epsilon S(t)}$. These two components are modeled by two (I_3 and I_2) current sources as shown in Fig.3.7. Thus, the light output is proportional to the output node in voltage representation. The voltage representation is applicable if transmission channel and receiver circuit are included in the simulation.

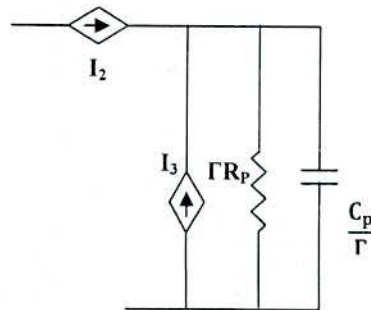


Fig.3.7. PSPICE circuit model of eqn. (3.63)

Now from Eqn. (3.62)-(3.63), the total equivalent circuit for a single QW laser obtained has been illustrated in Fig.3.8.

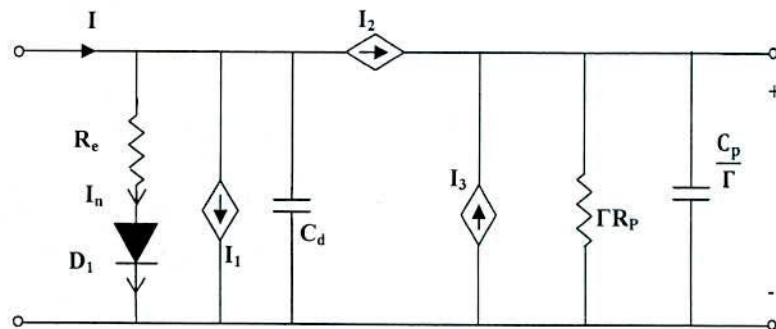


Fig.3.8. Equivalent circuit model of a single quantum well laser.

3.6 References

- [1] Peter M. Snowton, John D. Thomson, M. Yin, Susan V. Dewar, Peter Blood, A. Catrina Bryce, John H. Marsh, C. J. Hamilton, and C. C. Button, "The Effect of Cladding Layer Thickness on Large Optical Cavity 650-nm Lasers", IEEE Journal of Quantum Electronics, Vol. 38, No. 3, pp. 285-290, March 2002.
- [2] D.C.Liu, C.P. Lee, C.Pvl.Tsai, T.F.Lei, J.S.Tsang, W.H.Chiang, and Y.K.Tu, "Roll of cladding layer thicknesses on strained-layer InGaAs/GaAs single and multiple

- quantum well lasers”, *Journal of Applied Physics*, Vol. 73, No.12, pp. 8027-35, June 1993.
- [3] Shuji Nakamura, Masayuki Senoh, Shin-ichi Nagahama, Naruhito Iwasa, Takao Yamada, Toshio Matsushita, Yasunobu Sugimoto, and Hiroyuki Kiyoku, “Room-temperature continuous-wave operation of InGaN multi-quantum-well structure laser diodes with a lifetime of 27 hours”, *Applied Physics Letters*, Vol. 70, No. 1, pp. 1417-20 1997.
- [4] Takashi Matsuoka, “Progress in nitride semiconductors from GaN to InN—MOVPE growth and characteristics”, *Superlattices and Microstructures*, Vol. 37, No. 1, 19-32, January 2005.
- [5] V. Yu. Davydov, A. A. Klochikhin, V. V. Emtsev, S. V. Ivanov, V. V. Vekshin, F. Bechstedt, J. Furthmuller, H. Harima, A. V. Mudryi, A. Hashimoto, A. Yamamoto, J. Aderhold, J. Graul, and E. E. Haller, “Rapid Research Note Band Gap of InN and In-Rich $\text{In}_x\text{Ga}_{1-x}\text{N}$ alloys”, *Physica Status Solidi (b)* 230, No. 2, 2002.
- [6] Hongling Xiao, Xiaoliang Wang, Junxi Wang, Nanhong Zhang, Hongxin Liu, Yiping Zeng, and Jinmin Li, “Research on the band-gap of InN grown on silicon substrates”, *Physica Status Solidi (c)* 3, No. 3, pp. 594 – 597, 2006.
- [7] S. M. Thahab, H. Abu Hassan, Z. Hassan, “Performance and optical characteristic of InGaN MQWs laser diodes”, Vol. 15, No. 5, *Optics Express* 2380, pp. 2380-2390, March 2007.
- [8] Takashi Mukai, Motokazu Yamada and Shuji Nakamura, “Characteristics of InGaN-Based UV/Blue/Green/Amber/Red Light-Emitting Diodes”, *Japanese Journal of Applied Physics*, Vol. 38, pp. 3976–3981, 1999.
- [9] Yen-Kuang Kuo, Wen-Wei Lin and Jiann Lin, “Band-Gap Bowing Parameter of the $\text{In}_x\text{Ga}_{1-x}\text{N}$ Derived From Theoretical Simulation”, *Japanese Journal of Applied Physics*, 40, pp. 3157-3158, 2001.
- [10] Takahiro Numai, “Fundamentals of Semiconductor Lasers”, Springer-Verlag New York, Inc, ISBN 0- 387-40836-3, 2004.
- [11] Joachim Piprek, R. Kehl Sink, Monica A. Hansen, John E. Bowers, and Steve P. Den Baars, “Simulation and Optimization of 420 nm InGaN/GaN Laser Diodes”, *Physics and Simulation of Optoelectronic Devices VIII*, SPIE Proc. 3944, 2000.
- [12] M. Razeghi, and M. Henini, “Optoelectronic Devices: III-Nitrides”, Amanda Weaver Publisher, Elsevier Ltd.

- [13] S.C.P. Rodrigues, G.M. Sipahi, L.M.R. Scolfaro, J.R. Leite, "Valence-band structure of undoped and p-doped cubic GaN/InGaN multiple quantum wells", *Physica B*, Elsevier, Vol. 302–303, pp. 106–113, 2001.
- [14] V. Lemos, E. Silveira, J. R. Leite, A. Tabata, R. Trentin, "Evidence for phase-separated quantum dots in cubic InGaN layers from resonant Raman scattering", *Physical Review Letters*, Vol. 84, No. 16, pp. 3666–3669, 2000.
- [15] Li Shunfeng, Jorg Schormann, J. As. Donat and Klaus Lischka, "Room temperature green light emission from nonpolar cubic InGaN/GaN multi-quantum-wells", *Applied Physics Letter*, 90, pp. 071903-5, 2007.
- [16] Li Shunfeng, "Growth and characterization of cubic InGaN and InGaN/GaN quantum wells", 2005.
- [17] S. Berrah, A. Boukourt, and H. Abid, "The composition effect on the bowing parameter in the cubic InGaN, AlGaN and AlInN alloys", *Semiconductor Physics, Quantum Electronics & Optoelectronics*, Vol. 11, No 1, pp. 59-62, 2008.
- [18] Shun Lien Chuang, "physics of Optoelectronic Devices", Wiley-Interscience publication, ISBN 0-17 1-10939-8.
- [19] Supriyo Datta, "Quantum Transport: Atom to Transistor", Published in the United States of America by Cambridge University Press, New York, ISBN-13 978-0-511-1122-2.
- [20] Shun Lien Chuang, "Efficient band-structure calculations of strained quantum wells", *Physical Review B*, Vol. 43, No. 12, pp. 9651-63, April 1991.
- [21] Lucio Claudio Andreani, Alfredo Pasquarello and Franco Bassani, "Hole subbands in strained GaAs-Ga_{1-x}Al_xAs quantum wells: Exact solution of the effective-mass equation", *Physical Review B*, Vol 36, No 11, pp. 5887-94, October 1987.
- [22] M.M. Hasan, M.R. Islam, K. Teramoto, "Crystallographic orientation-dependent optical properties of GaInSb mid-infrared quantum well laser", *International Journal for Light and Electron Optics*, pp. 1-5, 2011.
- [23] Jasprit Singh, "qwkpvb-Quantum Well k.p Valence Subband Software USER'S MANUAL", Department of Electrical Engineering and Computer Science, University of Michigan, Ann Arbor, Michigan, January, 2003.
- [24] Shun Lien Chuang, "Optical Gain of Strained Wurtzite GaN Quantum-Well Lasers", *IEEE Journal of Quantum Electronics*, Vol. 32, No. 10, pp. 1791-1800, October 1996.
- [25] John P. Loehr and Jasprit Singh, "Theoretical Studies of the Effect of Strain on the Performance of Strained Quantum Well Lasers Based on GaAs and InP Technology", *IEEE Journal of Quantum Electronics*, Vol. 27, No. 3, pp. 708 –16, March 1991.

- [26] Peter John Stevens and Takaaki Mukai, "Predicted Performance of Quantum-Well GaAs-(GaAl)As Optical Amplifiers", IEEE Journal Of Quantum Electronics. Vol. 26, No. 11, pp. 1910 – 1917, November 1990.
- [27] Mohd Sharizal Alias, Burhanuddin Kamaluddin and Muhamad Rasat Muhamad, "1.55 μm Vertical-Cavity Lasers Modeling And Simulation", Solid State Science and Technology, Vol. 13, No 1 & 2, pp. 39-45, 2005.
- [28] M. Dehghan and V.Ahmadi, "Opto-Electro-Thermal Model for MQW Laser Including Self-Heating and Chirping effects", International Journal of Computer Science and Network Security, Vol.8, No.3, pp. 88-91, March 2008.
- [29] P. V. Mena, J. J. Morikuni, S.-M. Kang, A. V. Harton and K. W. Wyatt, "A Simple Rate-Equation-Based Thermal VCSEL Model", Journal of Lightwave Technology, Vol. 17, No. 5, pp. 865-72, May 1999.
- [30] R.S. Tucker & D.J.Pope, "Large Signal Circuit Model for Simulation of Injection-Laser Modulation Dynamics", IEEE Journal of Quantum Electronics, Vol. QE-19, pp. 1179-1183, July 1983.
- [31] D.M. Byrne, B.A Keating, "A laser diode model based on temperature dependent rate equations", IEEE Photonics Technology Letters, Vol. 1, No. 11, pp 356 – 359, 1989.
- [32] N. Bewtra, D.A. Suda, G.L. Tan, F.Chatenoud, J.M. Xu, " Modeling of quantum-well lasers with electro-opto-thermal interaction", IEEE Journal of Quantum Electronics, Vol. 1, No. 2, pp 331 – 340, Jun 1995.
- [33] A. Yurii Bumai, S. Aleh Vaskou, K. Valerii Kononenko, "Measurement and Analysis of Thermal Parameters and Efficiency of Laser Heterostructures and Light-Emitting Diodes", Metrology and Measurement Systems, Vol. XVII, pp. 39-46, 2010.
- [34] Gabor Farkas, Quint van Voorst Vader, Andras Poppe, and Gyorgy Bognar, "Thermal Investigation of High Power Optical Devices by Transient Testing", IEEE Transactions on Components and Packaging Technologies, Vol. 28, No. 1, March 2005.
- [35] R. S. Tucker and D. J. Pope, "Circuit modeling of the effect of diffusion on damping in a narrow-stripe semiconductor laser", IEEE Journal of Quantum Electronics, Vol. 19, No. 7, pp 1179-1183, 1983.
- [36] K. Hansen and A. Schlachetzki, "Transferred-electron device as a large-signal laser driver", IEEE Journal of Quantum Electronics, Vol. 27, No. 3, pp. 423-427, 1991.
- [37] Rodney S. Tucker, "Large-Signal circuit model for simulation of injection-laser modulation dynamics", IEE Proceedings on Solid-State and Electron Devices, Vol. 128, No. 5, pp. 180 – 184, October 1981.

SIMULATION RESULTS AND DISCUSSIONS

4.1 Introduction

Using the mathematical formulations presented in chapter III, the performance of the InGaN-based 1.55 μm quantum well heterostructure laser is evaluated in this chapter. It starts with the discussion of the results of band profile calculation, gain characterization, threshold current and bias voltage of the laser. This chapter includes the optimization of device parameters. The temperature effects on the characteristics are also included here. Most concern of this chapter is to discuss the results obtained from thermal and equivalent circuit modeling. The verifications of the proposed model with published results has been presented in this chapter. Finally, a comparative study on the models has been included.

4.2 Properties of InGaN QW Laser

The general properties of InGaN based quantum well edge emitting lasers like band structure analysis, gain nature, threshold properties, external differential quantum efficiency and internal quantum efficiency have been illustrated in this section.

4.2.1 Band Structure

We have calculated the subband energies for the conduction band (CI) and the valence bands (HH and LH) as a function of the InGaN well width. In the whole work, the effect of lattice mismatch and strain were not considered. In the InGaN quantum well, the conduction bands are assumed to be parabolic and the valence bands to be non parabolic. These bands have been computed by solving the Schrödinger equation using $\mathbf{k}\cdot\mathbf{p}$ method with a 4×4 Luttinger-Kohn Hamiltonian matrix operator. The physical parameters that have been used for simulations are listed in Table 4.1. These parameters like binary effective mass, lattice constants, elastic constants are linearly interpolated to obtain InGaN values from InN and GaN values using the following formula [1]

$$P(\text{In}_x\text{Ga}_{1-x}\text{N}) = xP(\text{InN}) + (1 - x)P(\text{GaN})$$

Table 4.1: The values of the parameters of InN and GaN used in the simulation model.

Parameter	Symbol	Unit	InN	GaN	References
Electron effective mass	m^*	m_0	0.11	0.20	[2]
Hole effective mass parameter	A_1	—	-9.24	-7.24	[2]
	A_2		-0.60	-0.51	
	A_3		8.68	6.73	
	A_4		-4.34	-3.36	
Lattice constants	a	Å	3.548	3.182	[3]
	c	Å	5.751	5.173	
Luttinger parameter	γ_1		3.72	2.70	[4-5]
	γ_2		1.26	0.76	
	γ_3		1.63	1.07	
Electron affinity	χ	eV	5.8	4.1	[6-7]
Thermal conductivity		(W/cmK)	0.45	1.3	[8-9]
Dielectric constant			15.3	8.9	[9]

In the analysis of QW structures using the $\mathbf{k}\cdot\mathbf{p}$ method for the calculation of the electronic band dispersion, a confining potential $V(z)$ along the growth direction z is added and k becomes an operator in the $\mathbf{k}\cdot\mathbf{p}$ Hamiltonian.

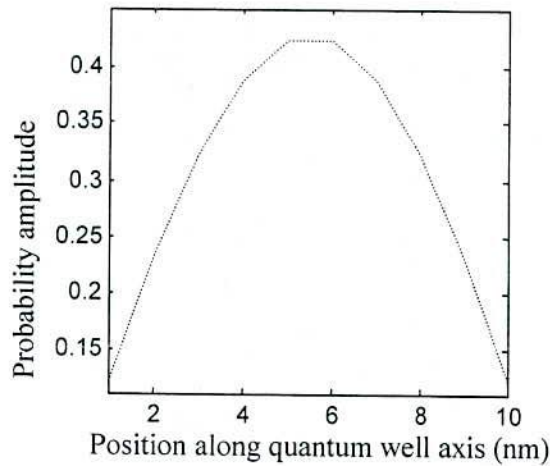


Fig.4.1. Probability distribution corresponding to the lowest eigen value.

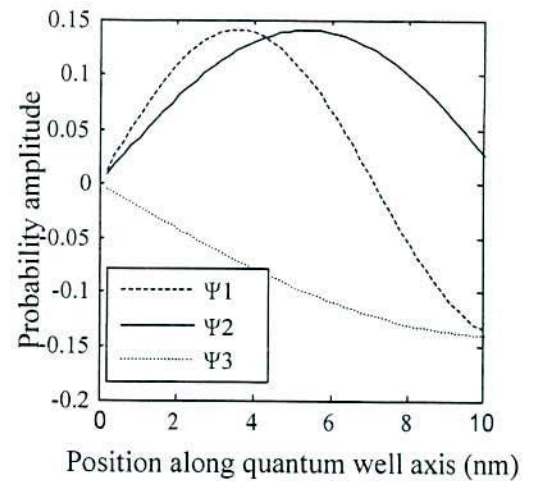


Fig.4.2. Probability distribution corresponding to the three eigen values.

The radial probability distribution (i.e. finding the electron in an orbital at any given distance away from the nucleus) tells us the probability of finding the electron in the volume of the

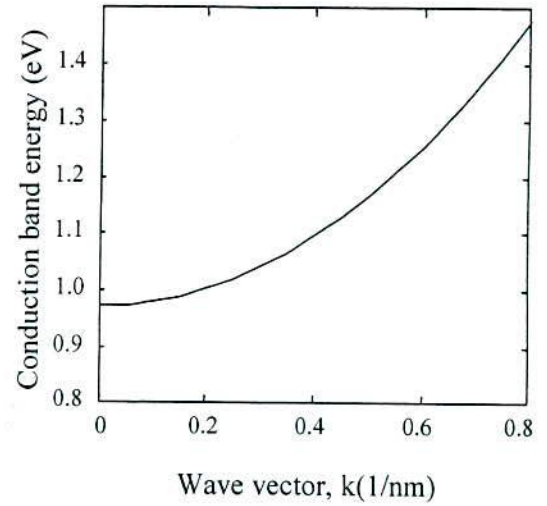
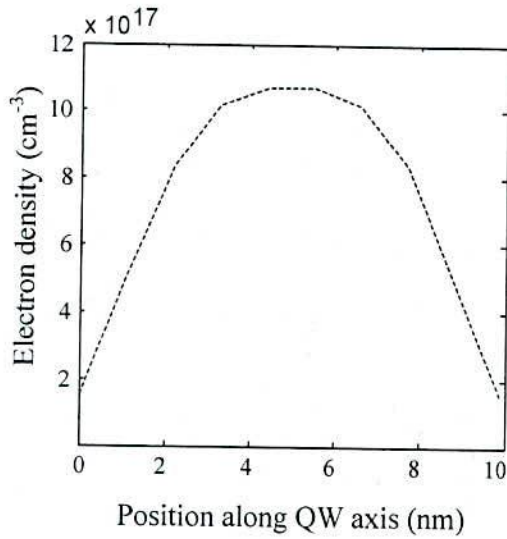


Fig.4.3. Electron density profile in conduction band. Fig.4.4. Energy of the first conduction subband (C1).

quantum well of the laser. Figure 4.1 and 4.2 show the probability distributions corresponding to the eigen values of the Hamiltonian of the time independent one dimensional Schrödinger equation for conduction subbands only. Figure 4.3 illustrates the electron density in the quantum well corresponding to the probability distribution mentioned in Fig.4.1. The electron density is found to be 10^{18} cm^{-3} and shown in Fig.4.3. The calculated conduction band dispersion profile is shown in Fig.4.4. Apart from the band edge ($k_t=0$), the energy is found to increase gradually with wave vector.

The valence band, heavy holes and light holes of InGaN based quantum wells have been considered in order to explain the mixing between the valence band states. In Fig.4.5 HH1, HH2, and HH3 indicate the first, second, and third heavy holes and LH1 is the first light hole. For any well length, the coupling between HH bands and the other kinds of bands is weak, hence the HH bands are nearly parabolic. The energies of the electron for the heavy-hole and light-hole subbands (Fig. 4.5) are plotted as a function of the wave number. We can see that the magnitudes of all energy levels decrease with the increase of wave number. It is found that the band mixing effect between heavy and light holes is less for our InGaN based lasers. These bands are in good agreement with the results presented by Piprek et al. [2].

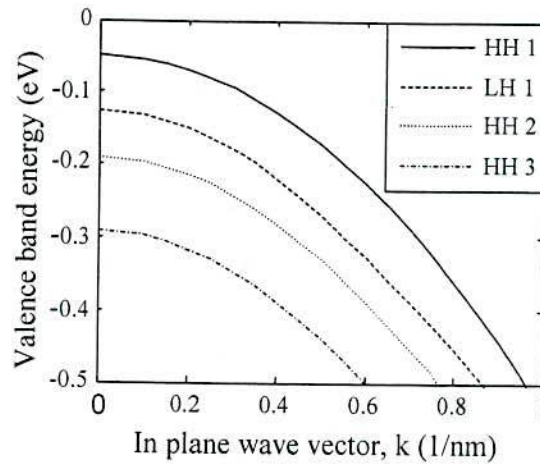


Fig.4.5. The valence subband dispersion functions of the first conduction and heavy hole bands of quantum well.

4.2.2 Gain of the Laser

Gain is an important parameter for the characterization of a laser. Optical gain, material gain and modal gain have significant influence on the investigation of the laser performance. The general parameters of InGaN quantum well laser used for the simulation model are given in Table 4.2.

Table 4.2: The InGaN parameters used in the simulation.

SL. No	Description of the parameters	Value of the parameters	Unit
01	Photon energy, $\hbar\omega$	0.85	eV
02	Active layer thickness, d	10	nm
03	Band gap energy of InGaN, E_g	0.8	eV
04	Temperature, T	300	K
05	Refractive index, n_r	3.35	-
06	Confinement factor, Γ	0.0035	-
08	Length of active layer, L	300	μm

Figure 4.6 shows the optical gain as a function of photon energy for InGaN based lasers. At low injections, f^e and f^h are quite small and the gain is negative. The f^e and f^h increase with the increase of injection for electrons and holes near band gap (0.8eV). As a result, the gain becomes positive with maximum value of 9000 cm^{-1} . The gain of this laser is higher than the GaAsSb/InGaNaNs/GaAs quantum well laser (5000 cm^{-1}) [10].

The threshold gain of the laser is the optical gain required for laser oscillation [11]. Oscillation is a state in which there is an output without an input from outside. The dependency of the threshold gain on the cavity length of the laser is shown in Fig.4.7. It is seen that for a cavity length of $300 \mu\text{m}$, the threshold optical gain is approximately 6 cm^{-1} .

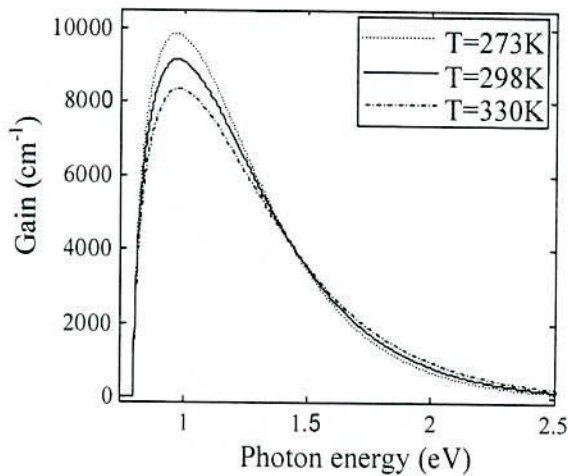


Fig.4.6. Optical gain vs. photon energy for InGaN based laser at different temperature.

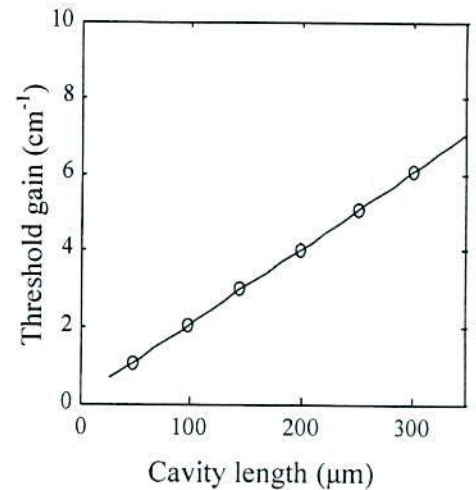


Fig.4.7. Threshold gain dependency of cavity length.

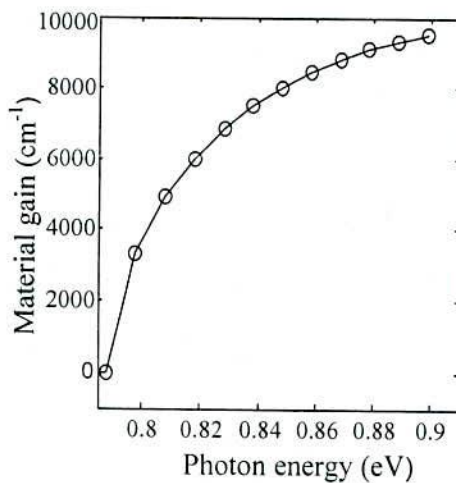


Fig.4.8. Material gain variation with photon energy.

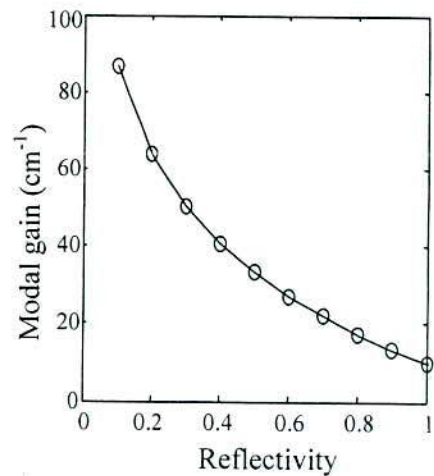


Fig.4.9. Modal gain variation with mirror reflectivity.

The material and modal gains are shown in Fig. 4.8 and 4.9 respectively. For photon energy greater than 0.8 eV, the material gain is about $3,660 \text{ cm}^{-1}$. For the device, we assume that, $R=35\%$, $L=300\mu\text{m}$ and $\alpha=20\text{cm}^{-1}$ [12], which forces modal gain, $\Gamma_g=45 \text{ cm}^{-1}$. Figure 4.9 shows that modal gain varies sharply with the change of the mirror reflectivity of partially transparent mirror. These results are comparable with Ma et al. [13] and Akram et al. [14].

4.2.3 Efficiency Analysis

External quantum efficiency and internal quantum efficiency for quantum well lasers are important for determining the number of photons emitted outside and inside the optical cavity

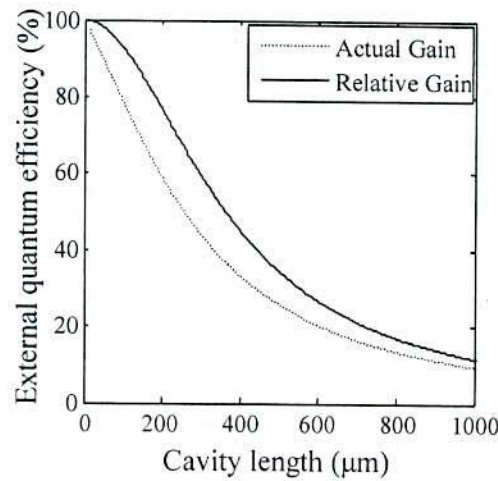


Fig.4.10. External quantum efficiency vs. cavity length, L.

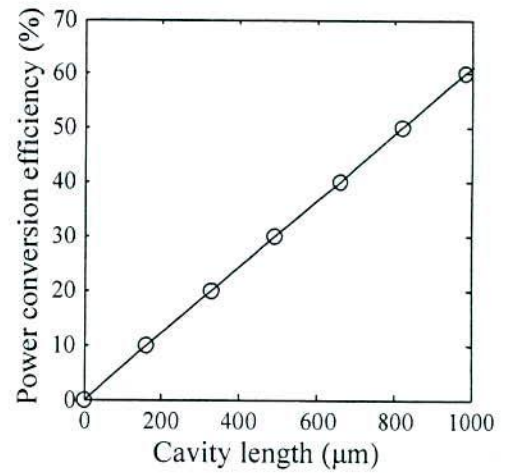


Fig.4.11. Power conversion efficiency vs. cavity length, L.

per injected carrier [3]. In Fig.4.10 the solid line indicates the relative efficiency while the dotted line shows the efficiency with considering waveguide loss (α_w) and the unavoidable signal shot noise loss (α_u). For a cavity length of $300\mu\text{m}$, the efficiency becomes 59% and 44% excluding and including waveguide loss (α_w) and the unavoidable signal shot noise loss (α_u) respectively. Figure 4.11 shows the variation of power conversion efficiency with the cavity length. For $300 \mu\text{m}$ cavity length the power conversion efficiency becomes 18% as shown in Fig.4.11. The internal quantum efficiency (η_i) is determined from the vertical axis intercept point ($1/\eta_i$) of the inverse external differential quantum efficiency (DQE) versus cavity length dependence linear fit line [15]. Figure 4.12 shows the calculation method for η_i with respect to the inverse value of DQE as a function of the cavity length. This gives approximately 94% internal quantum efficiency. It can be mentioned that the reported

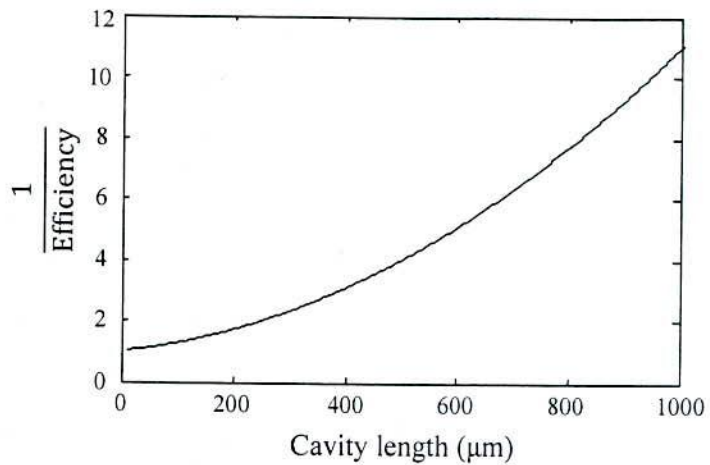


Fig.4.12. Inverse of the external quantum efficiency as a function of cavity length of QW InGaN laser.

external differential quantum efficiency is 50% [14,16] while the internal quantum efficiency is 58% [14]. These results are compatible with the results illustrated for our laser.

4.2.4 Output Characteristics

This section analyzes the electrical and optical output characteristics of the lasers. The current-voltage and output power-injection current characteristics are explained briefly.

4.2.4.1 I-V Characteristics Analysis

The I-V characteristic of InGaN 1.55 μm lasers at various temperatures is shown in Fig.4.13 by solid and dotted lines for three different temperatures of 0°C, 25°C and 53°C. The increase of applied voltage per degree rise of temperature is approximately 0.0074 volts only. It shows that I-V characteristics are less sensitive to temperature. The intrinsic carrier concentration changes with temperature, so the injection current changes. As the temperature rises, larger voltage is required to get a specific amount of injection current. From Fig.4.13 it is clear that the bias voltage 1.1 volts is required for appreciable current.

The threshold current density J_{th} as a function of the active layer thickness d is shown in Fig.4.14. The threshold current density increases with the increase of active layer thickness. The active layer thickness d , enhances confinement factor Γ which is proportional to d^2 . It is found that J_{th} has minimum value when d approximates to zero. It is noted that the threshold current density 1,119 Acm^{-2} is found for active layer thickness 10 nm for the proposed model.

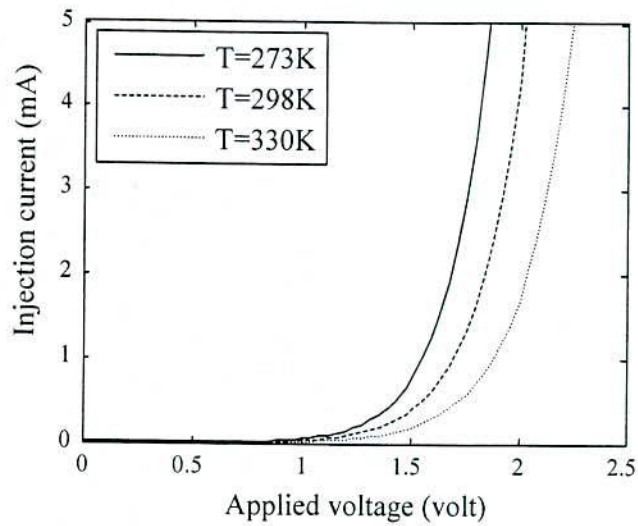


Fig.4.13. Current versus voltage (I-V) characteristics at different temperatures.

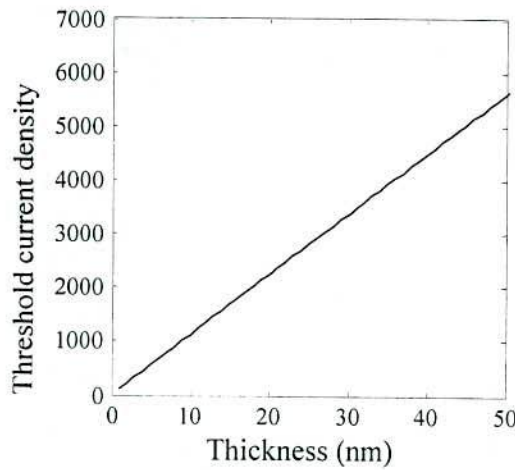


Fig.4.14. Dependence of the threshold current density, J_{th} on the active layer thickness.

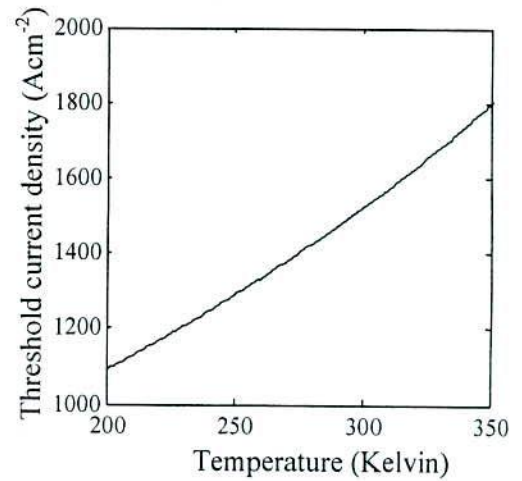


Fig.4.15. Dependence of the threshold current density, J_{th} on the temperature.

The variation of threshold current density with temperature is shown in Fig.4.15. It is observed that threshold current density increases with the increase of temperature. Thus, it needs high threshold current to obtain desirable gain at higher temperature. For this reason the laser with less temperature sensitivity is trying to develop in recent years. The higher characteristics temperature of InGaN substrate (intermediate layer) exhibits superior temperature characteristics than other ternary materials Laser. The threshold current density of our proposed laser is similar ($1.20\text{-}2.8\text{kAcm}^{-2}$) to reported in ref. [17]. These results show improved performance of the InGaN based lasers.

4.2.4.2 Optical Characteristics Analysis

The output power curve and slope efficiency of the QW laser diode are shown in Fig.4.16. It is seen that the output power varies linearly with injection current. The threshold current of 5.1mA is found from Fig.4.16. Below the threshold current, no light emits from the laser. It is mentioned that 3.0 mW output power is obtained at an injection current of 8.3mA. Slope value of 0.695W/A has been recorded at the laser threshold current.

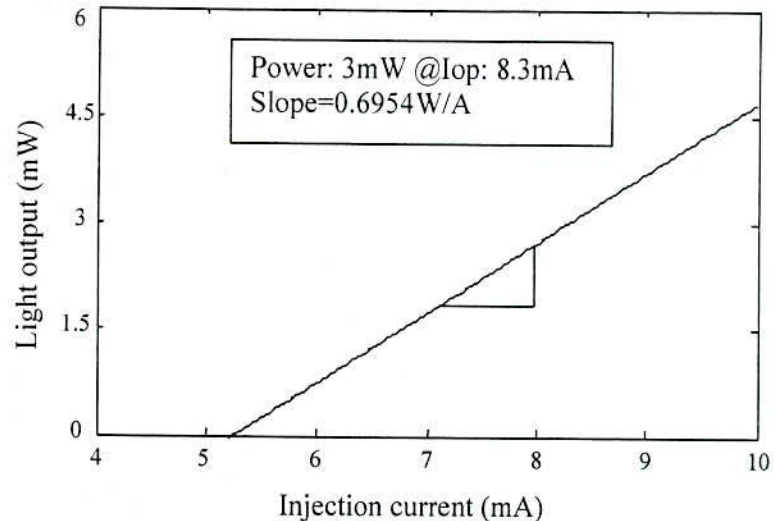


Fig.4.16. Output power from the laser vs. the injection current.

4.3 Thermal Effects on Threshold Current, Output and Power Efficiency

Thermal effects calculations are of immense important to understand the performance of the proposed laser at different operating conditions. The temperature dependency of the laser on the threshold current, optical power output and efficiency has been investigated in this article.

The behavior of output power-current (L-I) characteristics considering the thermal effect of InGaN based QW laser is shown in Fig.4.17. It is seen that the threshold current increases as well as the light output decreases at higher temperature. The maximum limit of output power is limited by injection current. It is also found from this figure that the injection current is changed by approximately 0.9 mA for each temperature difference of 10 °C. Thus, the laser's output is less sensitive to temperature.

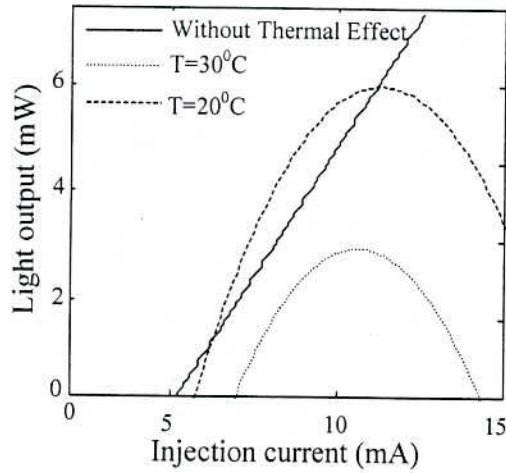


Fig.4.17. Temperature effect on L-I characteristics of InGaN based laser.

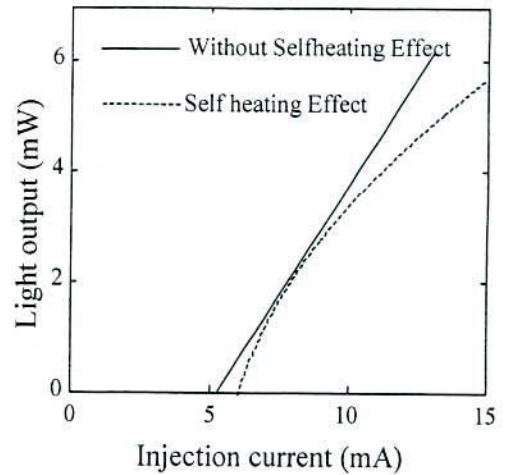


Fig.4.18. Self-heating effect on L-I characteristic of InGaN based lasers.

Figure 4.18 shows the L-I characteristics along with self-heating effect. It is found that more threshold current is required to emit light when self-heating effect is considered, as the increase in temperature of the active region causes degradation of photon emission. As illustrated in Fig.4.17 and 4.18, the simulation results are compared with the results obtained by neglecting thermal and self heating effects. Without these effects the output power increases linearly with the increase of injected current. The output power gets saturated when thermal effects have been considered. A significant change in threshold current is found excluding these effects.

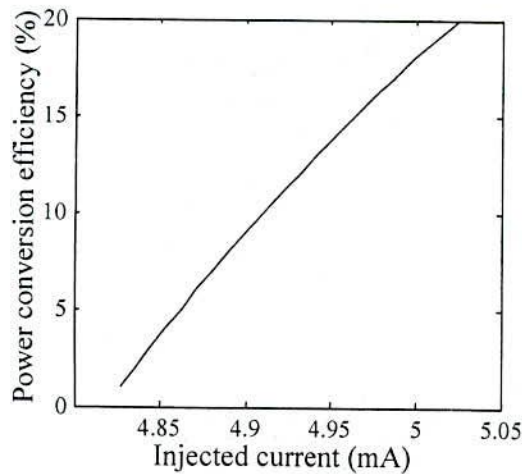


Fig.4.19. Power conversion efficiency vs. injection current.

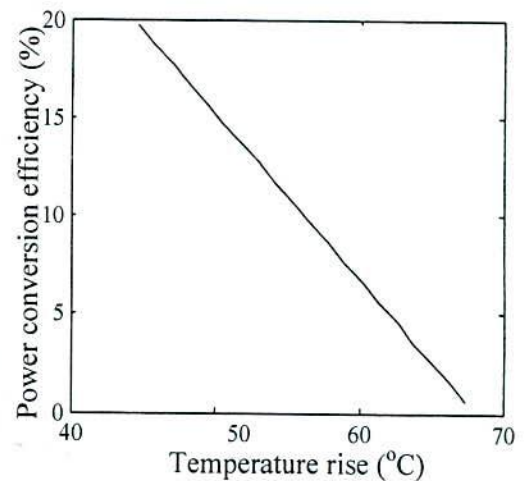


Fig.4.20. Temperature effect on power conversion efficiency.

The variation of laser power conversion efficiency with injection current and temperature is shown in Fig.4.19 and 4.20 respectively. The power conversion efficiency of InGaN based laser is dependent on injection current as well as temperature rise of the active region resulting from self-heating .A small increase in the injection current increases the efficiency sharply. It is seen from Fig.4.20 that the efficiency above 67 °C is almost zero due to sharp increase in junction and thermal resistance.

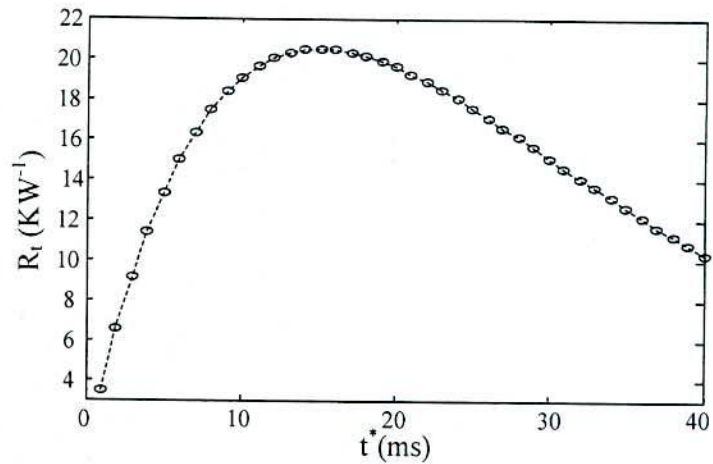


Fig.4.21. Thermal resistance variation with heat time constant.

Figure 4.21 shows the thermal resistance variation with heat time constant. The maximum value of the thermal resistance plot corresponding to the time scale gives the optimum value of thermal resistance, R_{Th} . The maximum points of R_t^* vs. τ^* curve shows the value of thermal resistance. Figure 4.21 determines the approximate maximum value of thermal resistance, R_{th} as $20KW^{-1}$.

4.4 PSPICE Circuit Simulation Results

Unlike electronic devices that are usually characterized by current and voltage, optoelectronic devices are normally characterized by light intensity and current. Since light intensity cannot be represented by any physical circuit quantities, modeling optoelectronic devices by PSPICE circuit model is certainly not physically transparent.

The results of PSPICE circuit model for InGaN based laser developed according to the electrical equivalent circuit discussed in section 3.5 is presented in this section. The parameters used for the PSPICE simulation taken from ref. [18] are given in Table 4.3.

Table 4.3: Parameters used in PSPICE circuit simulations.

Serial No.	Parameter	Unit	Value
1	R_e	Ω	0.468
2	R_p	Ω	29.4
3	R_s	Ω	2.0
4	τ_{ns}	ns	2.25
5	τ_{np}	ns	3
6	C_p	pF	0.102
7	C_d	pF	10
8	S_c	m^{-3}	10^{18}
9	D	$V^{-1}A^{-1}m^6$	1.79×10^{-29}
10	β_s	-	10^{-5}

The PSPICE circuit simulation evaluates the electrical characteristics such as current-voltage relationships, power output, turn on delay, and transient response of the laser equivalent circuit. Figure 4.22 shows the I-V response of the laser. It is seen that the current initiates to flow at an applied voltage of approximately 1.20 volts and then increases abruptly. The threshold value of the voltage is approximately 1.20 volts.

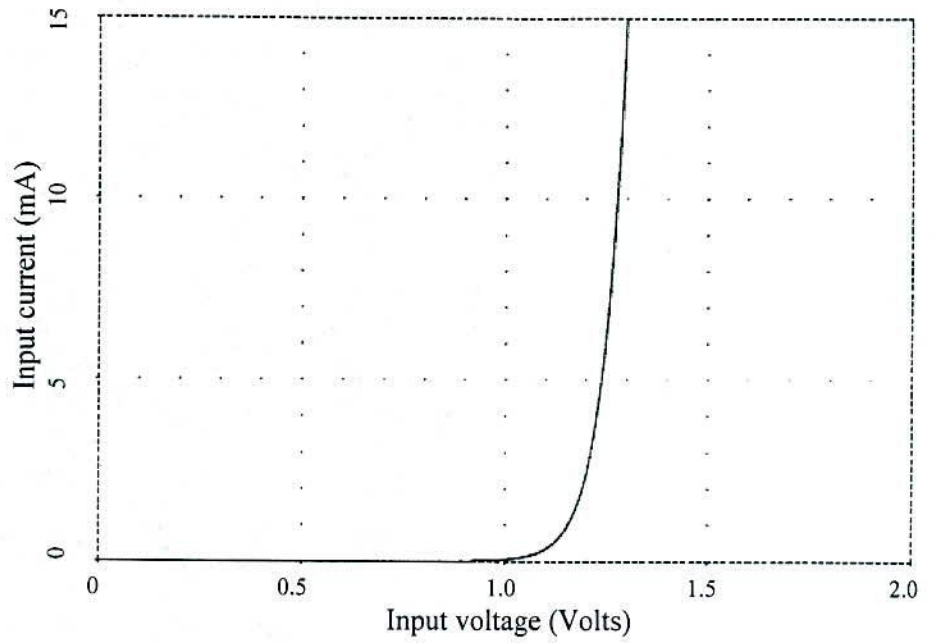


Fig.4.22. Current vs. voltage relationship for InGaN laser.

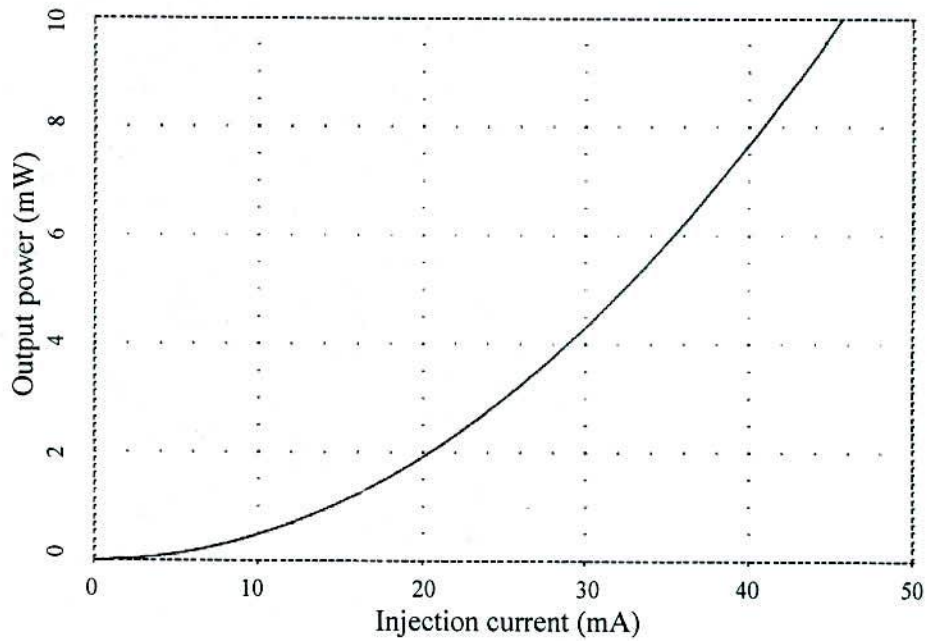


Fig.4.23. Output power-input current (L-I) characteristic of the proposed laser.

Figure 4.23 represents the output power with the variation of input current (L-I characteristics). The power output increases with the increase of input current. Threshold current of 6mA and the slope efficiency of approximately 0.368 W/A are found from Fig.4.23.

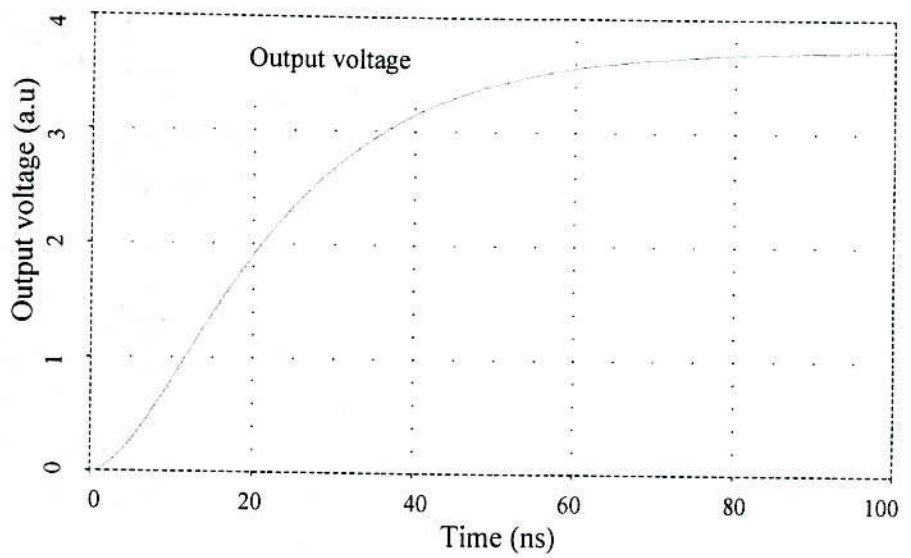


Fig.4.24. Output transient voltage of the laser.

The transient response of the laser is shown in Fig.4.24. The steady state values of output voltage are found after 60ns. Turn on delay of 3ns is calculated from Fig.4.25 for InGaN based laser. These results show the consistency with the results obtained from the previous discussions.

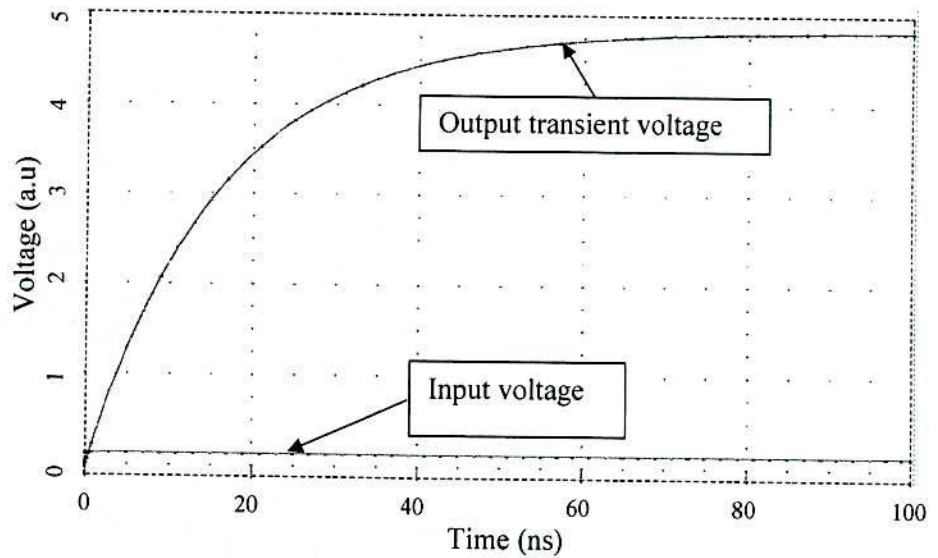


Fig.4.25. Turn on delay time.

4.5 Comparison of Results

From the earlier studies of the InGaN based laser it is necessary to show a comparative clarification of the results. The general characterization of the laser shows the threshold current of 5.1 mA, bias voltage of 1.1 volts and slope efficiency of current-power output (L-I) curve of 0.695 W/A. It is found that 3.0 mW output power is obtained at an injection current of 8.3mA at room temperature. Thermal modeling of laser also illustrates that the threshold current of about 5.5 mA, slope efficiency of 0.61 W/A and a power output of 3mW at an injection current of approximately 7.5mA at same ambient temperature. Furthermore, the equivalent circuit modeling shows the threshold current of 6 mA and bias voltage of 1.20 volts. Slope efficiency of 0.368 W/A has been found from the L-I characteristics curve. Power output of 3mW has been found at an injection current of 25mA. This show a difference with the result from general analysis as the change in circuit parameters are not similar to that of calculations adopted in analytical method. Therefore, the above discussions show the consistency of the proposed model.

4.6 Verification

InGaN based lasers are very much immature. Thahab et al. [15, 19] and Piprek et al. [2, 20] described the performance and optical characteristic for long wavelengths (420nm) of InGaN/GaN laser diodes. For shorter wave lengths Sandra et al. [21] and Alias et al. [22] studied the laser performance using InGaAsP and AlGaInAs/InP respectively. Theoretical and experimental study on InGaN based lasers is still necessary. To justify the validity of the proposed 1.55 μm lasers the results obtained from the simulations are required to verify and compare with the published results. The detail simulation results for InGaN based lasers have been shown in Table 4.4 and a comparison with reference work has been presented also.

The electronic band calculation of the laser has been performed by solving one dimensional time independent Schrödinger equation. The energy profiles of the conduction band and valence sub bands are agreed to that of ref. [21, 23-24]. The calculated electron concentration (10^{18}cm^{-3}) is similar as reported in [19]. This indicates that our proposed model can reasonably calculate the energy band profiles.

In this study we found high gain ($9,000\text{cm}^{-1}$), moderate material gain ($3,660\text{cm}^{-1}$) and modal gain (45cm^{-1}) of the laser. It is seen (Table 4.4) that threshold current density ($1,119\text{Acm}^{-2}$), and threshold current (5.1mA) are lower than published values. It is also found the improved external differential quantum efficiency (59%) and internal quantum efficiency. From the

above study it is clear that our achievements are better than some reports and are comparable to others which proves the validation of the proposed model.

Table 4.4: Detail simulation results of InGaN based laser.

Sl. No.	Parameter	Present Work	Reference Work	Reference
1	Optical Gain	9000 cm⁻¹	5000cm ⁻¹ 8000cm ⁻¹	[10] [13]
2	Material Gain	3600 cm⁻¹	1950cm ⁻¹	[13]
3	Modal Gain	45 cm⁻¹	32cm ⁻¹	[14]
	Threshold Current, I _{th}	5.1mA	7.5mA 15mA 7.9mA 17.8mA	[14] [16] [25] [26]
4	Threshold Current Density, J _{th}	1.8kA cm⁻²	4kAcm ⁻² 1.06 kAcm ⁻²	[16] [17]
6	Slope of L-I curve	0.696W/A	0.301W/A 0.35W/A	[25] [26]
7	External Quantum Efficiency, η _d	59%	38% 50% 31% 50%	[14] [16] [17] [27]
9	Internal Quantum Efficiency, η _i	94%	58	[14]

4.7 References

- [1] Shun Lien Chuang, "Physics of Optoelectronic Devices", Wiley-Interscience publication, ISBN 0-17 1-10939-8.
- [2] Joachim Piprek and Shuji Nakamura, "Physics of high-power InGaN/GaN lasers", IEE Proceedings of Optoelectronics, Vol. 149, No. 4, pp. 145 – 151, August 2002.
- [3] Qimin Yan, Patrick Rinke, M. Winkelnkemper, A. Qteish, D. Bimberg and Matthias Scheffler, "Band parameters and strain effects in ZnO and group-III nitrides", Semiconductor Science and Technology, Vol. 26, No. 1, pp. 1-8, 2011.
- [4] Shuji Nakamura and Shigefusa F. Chichibu, "Introduction to Nitride Semiconductor Blue Lasers and Light Emitting Diodes", CRC Press, New York, ISBN 0-7484-0836-3.
- [5] Hadis Morkoc, "Handbook of Nitride Semiconductors and Devices: Materials properties", Vol. 1, Material Properties, Physics and Growth, ISBN 978-3-527-40837-5.

- [6] V. Bougrov, M.E. Levinshtein, S.L. Rumyantsev, A. Zubrilov, "Properties of Advanced Semiconductor Materials GaN, AlN, InN, BN, SiC, SiGe", John Wiley & Sons, Inc., New York, 2001.
- [7] J. W. Ager, N. Miller, R. E. Jones, K. M. Yu, J. Wu, W. J. Schaff, and W. Walukiewicz, "Mg-doped InN and InGaN-Photoluminescence, capacitance-voltage and thermo power measurements", *Physica Status Solidi (b)* 245, No. 5, pp. 873–877, 2008.
- [8] S. Krukowski, A. Witek, J. Adamczyk, J. Jun, M. Bockowski, I. Grezegory and Zinn, "Thermal properties of Indium Nitride", *Journal of Physics and Chemistry of Solids*, Vol 59, No. 3, pp. 289-295, 1998.
- [9] M. Razeghi, and M. Henini, "Optoelectronic Devices: III-Nitrides", Amanda Weaver Publisher, Elsevier Ltd.
- [10] Seoung-Hwan Park, "Optical Gain of Type-II 1.55- μm GaAsSb/InGaAs/GaAs Trilayer Quantum Wells", *Journal of the Korean Physical Society*, Vol. 53, No. 4, pp. 1886-1890, October 2008.
- [11] Doyeol Ahn and Tae-Kyung Yoo, "Envelope Function Calculations of Linear and Nonlinear Optical Gains in a Strained-Layer Quantum-Well Laser", *IEEE Journal of Quantum Electronics*, Vol. 29, No. 12, pp. 2864 – 2872, December 1993.
- [12] Takahiro Numai, "Fundamentals of Semiconductor Lasers", Library of Congress, ISBN 0-387-40836-3, Springer-Verlag New York, Inc. 2004.
- [13] T.-A. Ma, Z.-M. Li, T. Makino, and M. S. Wartak, "Approximate Optical Gain Formulas for 1.55- μm Strained Quaternary Quantum-Well Lasers", *IEEE Journal of Quantum Electronics*, Vol. 31, No. 1, pp. 29 – 34, January 1995.
- [14] M. Nadeem Akram, O. Kjebon, M. Chacinski, R. Schatz, J. Berggren, F. Olsson, S. Lourudoss, and A. Berrier, "Experimental characterization of high-speed 1.55 μm buried heterostructure InGaAsP/InGaAlAs quantum-well lasers", *Journal of the Optical Society of America B*, Vol. 26, No. 2, pp 318, February 2009.
- [15] S. M. Thahab, H. Abu Hassan, and Z. Hassan, "Performance of InGaN/GaN Laser Diode Based on Quaternary Alloys Stopper and Superlattice Layers", *World Academy of Science, Engineering and Technology* 55, pp. 11-14, 2009.
- [16] G. Almuneau, F. Genty, A. Wilk, P. Grech, A. Joulli and L. Chusseau, "GaInSb/AlGaAsSb strained quantum well semiconductor lasers for 1.55 μm operation", *Semiconductor Science and Technology*, Vol. 14, pp. 89–92, 1999.
- [17] S.R. Bank, M.A. Wistey, L.L. Goddard, H.B. Yuen, V. Lordi, J.S Harris, "Low-threshold continuous-wave 1.5- μm GaInAsSb lasers grown on GaAs", *IEEE Journal*

- of Quantum Electronics, Vol. 40, No. 6, pp. 656 – 664, June 2004.
- [18] M. F. Lu, J. S. Deng, C. Juang, M. J. Jou, and B. J. Lee, “Equivalent Circuit Model of Quantum- Well Lasers”, IEEE Journal of Quantum Electronics, Vol. 31, No. 8, pp. 1418-22, August 1995.
- [19] S. M. Thahab, H. Abu Hassan, Z. Hassan, “Performance and optical characteristic of InGaN MQWs laser diodes”, Vol. 15, No. 5, Optics Express 2380, pp. 2380-2390, March 2007.
- [20] Joachim Piprek, R. Kehl Sink, Monica A. Hansen, John E. Bowers, and Steve P. DenBaars, “Simulation and Optimization of 420 nm InGaN/GaN Laser Diodes”, Physics and Simulation of Optoelectronic Devices VIII, SPIE Proc. 3944, 2000.
- [21] Sandra R. Selmic, Tso-Min Chou, JiehPing Sih, Jay B. Kirk, Art Mantie, Jerome K. Butler, David Bour, and Gary A. Evans, “Design and Characterization of 1.3- μm AlGaInAs–InP Multiple-Quantum-Well Lasers”, IEEE Journal of Selected Topics in Quantum Electronics, Vol. 7, No. 2, pp. 340 – 349, March/April 2001.
- [22] Mohd Sharizal Alias, Burhanuddin Kamaluddin and Muhamad Rasat Muhamad, “1.55 μm Vertical-Cavity Lasers Modeling and Simulation”, Solid State Science and Technology, Vol. 13, No 1 & 2, pp. 39-45, 2005.
- [23] Lucio Claudio Andreani, Alfredo Pasquarello and Franco Bassani, “Hole subbands in strained GaAs-Ga_{1-x}Al_xAs quantum wells: Exact solution of the effective-mass equation”, Physical Review B, Vol. 36, No 11, pp. 5887-5894, 1987.
- [24] D. L. Smith and C. Mailhot, “Theory of semiconductor superlattice electronic structure”, Reviews of Modern Physics, Vol. 62, No. 1, pp. 173-234, January 1990.
- [25] T. Yamamoto, K. Takada, M. Matsuda, S. Okumura, S. Akiyama, and M. Ekawa, “1.55- μm -Wavelength AlGaInAs Multiple-Quantum-Well Semi-Insulating Buried-Heterostructure Lasers”, IEEE 20th International Conference on Semiconductor Laser, pp. 15-16, 2006.
- [26] Bo-Ting Liou, Sheng-Horng Yen, Ming-Wei Yao, Mei-Ling Chen, Yen-Kuang Kuo, Shu-Hsuan Chang, “Numerical study for 1.55- μm AlGaInAs/InP semiconductor lasers”, Proceedings on Optoelectronic Devices: Physics, Fabrication, and Application III Vol. 6368, October 2006.
- [27] S.R. Bank, M.A. Wistey, L.L. Goddard, H.B. Yuen, V. Lordi, J.S Harris, “Low-threshold CW GaInNAsSb/GaAs laser at 1.49 μm ”, IEEE Electronics Letters, Vol. 39 No. 20, pp.1445 – 1446, October 2003.

CONCLUSIONS AND FUTURE WORK

5.1 Conclusions

The modern ultra speed communication systems has provided a possibility to the study about 1.55 μm lasers because of their well matched and sustainability with the existing fiber optic infrastructures. These lasers are also posse's substantially lower attenuation, transmission losses, waveform degradation, and dispersion penalty. The goal of this work was to develop a high performance InGaN based 1.55 μm quantum well edge emitting laser. In this thesis the physical model of the laser structure is proposed. Then the mathematical model of the laser is developed solving Schrödinger and Poisson's equation with the help of finite difference method.

The simulation and analysis results for band structure of the quantum well laser reveal the energy separation between different band and subbands for quantum well laser. It is observed that the electron density in conduction band is 10^{18}cm^{-3} . The understanding of the characteristics of the laser, parameters such as threshold current, gain, applied bias voltage, efficiency, light output are of immense important for successful laser fabrication. These parameters evaluate the performance of the laser. The effects of active layer thickness on the threshold current density and optical confinement factor in the quantum well laser have been investigated. The threshold current density, $1,119\text{A}/\text{cm}^2$ and the optical confinement factor, 0.0035 for active layer thickness 10nm, are obtained. External quantum efficiency of 59% has been found keeping the reflectivity at 35% of one mirror and 100% of other. It is seen that efficiency increases with the decrease of reflectivity. This efficiency reduces to 44% when the waveguide and the unavoidable signal shot noise losses are considered for the same reflectivity. The internal efficiency of 94% and slope efficiency of $0.695\text{W}/\text{A}$ has been found. In addition, a very small threshold current (5.1mA) is obtained to emit light that requires lower applied voltage of 1.10 volts. Finally, the output power (5mW), high optical gain ($9,000\text{cm}^{-1}$), moderate material gain ($3,660\text{cm}^{-1}$) and modal gain (45cm^{-1}) have been found.

In order to achieve progress in the applicability of InGaN based laser under different ambient temperatures the thermal effects analysis is imperative. It is found that the threshold current has been increased to 5.5mA at the same ambient temperature. The laser efficiency strongly depends on the injection current and has small effect on temperature. The thermal resistance 20KW^{-1} is calculated from this model. It is seen that the proposed laser is less temperature sensitive and self heating effect have little effect on the laser performance.

In addition, to understand the performance of the proposed laser it is very important to study its output characteristics. These characteristics are realized through the development of the equivalent circuit modeling of the quantum well laser. The PSPICE circuit simulation shows that the output power increases with the increase of input current. Threshold current of approximately 6 mA, bias voltage of 1.20 volts, slope efficiency of 0.368W/A and turn on delay of 3ns have been found from this circuit analysis. These electrical characteristics show consistency with the results obtained from performance analysis and thermal modeling.

Therefore, the study presented in this thesis indicates the potentiality of the InGaN based quantum well laser for the promising device in the field of modern optoelectronics.

5.2 Future Works

The research described in this thesis was concerned with the theoretically design, band structure calculation, thermal modeling and equivalent circuit modeling of InGaN-based $1.55\mu\text{m}$ quantum well lasers. The proposed lasers have been successfully designed with many exciting results. These have created the way for future work with a goal to fabricate practical InGaN based high performance $1.55\mu\text{m}$ lasers. There are many areas where future research is required. The works remaining for future study are discussed as follows.

The efficiency of the laser can further increase by using multi quantum well. By the appropriate use of wells number and its barriers thickness, more carriers might confine and efficiency may increase. The effect of strain and stress on quantum well lasers has significant effect. There has scope on the work to analyze the strain dependent and crystal orientation dependent optical properties, piezoelectric effect of InGaN based lasers. In band profile calculation one dimensional Schrödinger equation and conduction band, heavy holes and light holes have been considered. Two dimensional calculations may be implemented of the laser structure for more accurate results. The Hamiltonian matrix elements can be increased to determine spin split-off bands. Future work can be extended on the investigation of device life time, determining transition time and so on.

List of Publications

International journals:

- [1] **Md. Jahirul Islam**, Md. Rafiqul Islam, "Design and Gain Analysis of 1.55 μm Laser Using InGaN", International Journal of Electronics and Computers, Vol. 3, No. 1, January-June 2011.
- [2] Md. Tanvir Hasan, **Md. Jahirul Islam**, Rajib-ul-Hasan, Md. Sherajul Islam, Shahrina Yeasmin, Ashraful G. Bhuiyan, Md Rafiqul Islam, and Akio Yamamoto, "Design and performance of 1.55 μm laser using InGaN", Phys. Status Solidi C, Vol. 7, No. 7-8, 2010.

International Conference Papers:

- [3] **Md Jahirul Islam**, Md. Rafiqul Islam, Md. Mottaleb Hossain, "Design and Characterization of InGaN Based 1.55 μm Lasers Using Thermal Modeling", International Conference on Advances in Electrical Engineering, (ICAEE 2011), Independent University, December 19-20, Bangladesh, 2011.
- [4] **Md. Jahirul Islam**, Md Rafiqul Islam, "Design and Gain Analysis of 1.55 μm Laser Using InGaN", International Conference on Emerging Technologies(ICET), Durgapur, India, 2011.
- [5] Md. Tanvir Hasan, **Md. Jahirul Islam**, Rajib-ul-Hasan, Md. Sherajul Islam, Shahrina Yeasmin, Ashraful G. Bhuiyan, Md Rafiqul Islam, and Akio Yamamoto "Design and performance of 1.55 μm laser using InGaN", ICNS conference, Korea, 2010.